

Probing Calmodulin-NO Synthase Interactions via Site-Specific Infrared Spectroscopy: An Introductory Investigation

| Journal: | Journal of Biological Inorganic Chemistry |
|-------------------------------|--|
| Manuscript ID | JBIC-23-11-00189.R1 |
| Manuscript Type: | Original Paper |
| Date Submitted by the Author: | 11-Jan-2024 |
| Complete List of Authors: | Singh, Swapnil; Indiana University, Chemistry Gyawali, Yadav; University of New Mexico, College of Pharmacy Jiang, Ting; University of New Mexico College of Pharmacy, Pharmaceutical Sciences Bukowski, Gregory; Indiana University, Chemistry Zheng, Huayu; University of New Mexico, College of Pharmacy Zhang, Haikun; University of New Mexico, College of Pharmacy Owopetu, Rebecca; University of New Mexico College of Pharmacy, Pharmaceutical Sciences Thielges, Megan; Indiana University, Chemistry Feng, Changjian; University of New Mexico, College of Pharmacy |
| Keywords: | nitric oxide synthase, calmodulin, p-cyano-L-phenylalanine, transparent window FT IR spectroscopy |
| | |

SCHOLARONE™ Manuscripts

Probing Calmodulin-NO Synthase Interactions via Site-Specific Infrared Spectroscopy: An Introductory Investigation

Swapnil Singh^{‡a}, Yadav Prasad Gyawali^{‡b}, Ting Jiang^b, Gregory S Bukowski^a, Huayu Zheng^b,

Haikun Zhang^b, Rebecca Owopetu^b, Megan C Thielges^{*a}, Changjian Feng^{*b}

aDepartment of Chemistry, Indiana University, Bloomington, Indiana 47405, United States

bDepartment of Pharmaceutical Sciences, University of New Mexico, Albuquerque, New Mexico

87131, United States

Corresponding Authors

* Changjian Feng – College of Pharmacy,

University of New Mexico, Albuquerque, New Mexico 87131,

United States; orcid.org/0000-0003-4542-6497;

Email: cfeng@unm.edu

* Megan C. Thielges – Department of Chemistry, Indiana University, Bloomington, Indiana 47405, United States;

orcid.org/0000-0002-4520-6673; Email: thielges@iu.edu

Author Contributions

‡S.S and Y.P.G contributed equally.

Abstract

Calmodulin (CaM) binds to a linker between the oxygenase and reductase domains of nitric oxide synthase (NOS) to regulate the conformational dynamics. Specific residues on the interdomain interface guide the domain-domain docking to facilitate the electron transfer in NOS. Notably, the docking interface between CaM and the heme-containing oxygenase domain of NOS is isoformspecific, which is only beginning to be investigated. Toward advancing understanding of the distinct CaM-NOS docking interactions by infrared spectroscopy, we introduced a cyano group as frequency-resolved vibrational probe in CaM individually and when associated with full-length and an oxygenase/FMN construct of the inducible isoform iNOS. Selective labeling with p-cyano-L-phenylalanine (CNF) by amber suppression of CaM bound to the iNOS has been accomplished by protein coexpression due to the instability of iNOS alone. We introduced a cyano at residue 108, which is at the putative CaM-NOS docking interface. CNF also was introduced at residue 29, which is distant from the CaM-heme(NOS) docking interface. FT IR data indicate that the 108 site is sensitive to CaM-NOS complex formation, while insensitivity to its association with the iNOS protein or peptide was observed for the 29 site. Moreover, narrowing of the IR bands at residue 108 suggests the C≡N probe experiences a more limited distribution of environments, indicating side chain restriction apparent for the complex with iNOS. This work set the stage for residuespecific characterizations of structural dynamics of the NOS docked states.

KEYWORDS: nitric oxide synthase, calmodulin, *p*-cyano-L-phenylalanine, transparent window FT IR spectroscopy

Abbreviations

NOS, nitric oxide synthase; iNOS, inducible NOS; nNOS, neuronal NOS; eNOS, endothelial NOS; CaM, calmodulin; oxyFMN, bidomain oxygenase/FMN construct in which only the oxygenase and FMN domains are present, along with the CaM binding region; CNF108 CaM, CNF is introduced at 108 site on helix G within the C-lobe; CNF29 CaM, CNF is introduced at 29 site on helix B within the N-lobe; p-NOS, peptide containing the CaM binding region of NOS.

Introduction

Nitric oxide synthase (NOS) catalyzes the conversion of L-arginine to nitric oxide (NO), a signaling molecule with important roles in diverse physiological processes.¹⁻⁴ Aberrant NOS activity contributes to numerous diseases, including cardiovascular disease, neurological disorders, and inflammatory conditions.⁵⁻⁹ There are three mammalian NOS isoforms: neuronal, endothelial, and inducible NOS (nNOS, eNOS, and iNOS, respectively). The nNOS and eNOS isoforms are constitutively expressed. Knowledge of the regulation mechanisms of NOS isoforms is essential for both advancing our understanding of fundamental biological processes and for developing targeted therapeutics for a range of diseases.

Mammalian NOS is a homodimeric protein, with each subunit containing an N-terminal catalytic heme-containing oxygenase domain and a C-terminal reductase domain. The reductase domain itself is composed of FMN- and NADPH/FAD-binding subdomains. ¹⁰⁻¹³ Catalytic throughput is governed by interdomain electron transfer in which the FMN subdomain acts as an electron shuttle, interacting alternatingly with the NADPH/FAD subdomain (electron-accepting input state) and the oxygenase domain (electron-donating output state). ¹⁴⁻²⁰ Transition between the input and output states requires large-scale conformational changes that are controlled by binding of calmodulin (CaM) to a ~ 30-amino acid region connecting the oxygenase and FMN domains. ^{21, 22} Compelling evidence shows the importance of interdomain docking in the regulation of NOS by CaM. ^{23, 24} Moreover, we have recently demonstrated that, in contrast to the FMN/heme interface, ²⁵ the CaM/heme interface is isoform-specific, ²⁶ which remains underexplored. Notably, there is an urgent need to develop new intervention strategies selectively targeting different NOS isoforms, as a clinical NOS inhibitor is lacking.

Association of CaM with NOS modulates the conformational dynamics between the input and output states and thereby catalytic throughput, ^{14, 16, 27-29} but the full details of the mechanism and how it varies among the isoforms remain unclear. A challenge to elucidating the isoform-specific mechanisms of CaM recognition and regulation of NOS is the enzyme's heterogeneous and dynamic nature, involving at least three distinct conformational states (input, output, and free/open states) mediated by domain-domain interactions. Mounting evidence supports the mechanism that large-scale tethered FMN domain motion plays a key role in NOS function by bringing the electron transfer modules in close proximity. Moreover, local conformational adjustments occurring on relatively fast timescales continue in the docked domain-domain complex states. A comprehensive picture will remain missing without detailed insight into the docked state. This information is crucial to elucidating the interplay between dynamics and function.

As a foundational step in our systematic investigation of the NOS regulatory dynamics by CaM, herein we apply residue-selective vibrational spectroscopy toward elucidating the CaM-NOS docked states. A cyano ($C\equiv N$) group was introduced as a vibrational probe of specific locations in CaM. The $C\equiv N$ group absorbs in a transparent spectral window of congested protein IR spectra to enable its absorption to be distinctly detected and analyzed. IR spectral analysis informs about the probe's local environment(s) and thus can illuminate the residue's involvement in molecular recognition. We chose to incorporate a genetically coded IR probe (e.g., cyano or azide) in CaM instead of NOS, since CaM is smaller and overexpresses better in various plasmids and *E. coli* strains. Indeed, CaM is amenable to incorporation of *p*-azido-phenylalanine (AzF), an IR sensor. AzF gives a stronger signal than *p*-cyano-L-phenylalanine (*CN*F), but interpretation of its IR spectra is complicated by Fermi resonances.

Results and Discussion

We first generated *CNF*-labelled CaM, along with *CNF* CaM co-expressed with human iNOS protein. IR spectroscopy was then applied to characterize the *CNF* probe in CaM individually, when associated with an iNOS protein, and, for comparison, when associated with a peptide containing the cognate NOS linker sequence with which CaM associates (p-iNOS; see **Table S3**).^{22,33} We utilized an oxyFMN construct in which only the oxygenase and FMN domains along with the CaM binding sequence are present.³⁴ This was done to enhance the FMN-heme domain docking probability and to facilitate the study of CaM-heme docking interfaces. Note that in the full-length protein, the NAPDH/FAD subdomain competes with the heme domain to interact and dock with the FMN subdomain. Furthermore, we analyzed full-length iNOS protein in complexation with the *CNF* labelled CaM to a) examine the potential impact of the NADPH/FAD subdomain on the CaM-heme docking interactions and b) validate the oxyFMN results.

Regarding the labeling site, we substituted *CNF* in a position that: a) shows a different degree of solvent exposure in Ca²⁺-CaM compared to Ca²⁺-CaM in complex with NOS, and b) is adjacent to the CaM residues interacting with the isoform-specific NOS residues.³⁵ We directed the CaM labeling based on the docking models of an iNOS oxyFMN construct.^{36, 37} For example, Val108 has a different degree of solvent exposure in the CaM-NOS complex than in CaM alone sample (**Figure 1**)³⁸. Val108 is also near Arg106 within an electrostatic patch adjacent to the putative CaM-heme(NOS) docking interface, which is variable among NOS isoforms.³⁶ As such, Val108 should be sensitive to CaM-NOS complex formation. As a control, we introduced *CNF* on helix B at solvent-exposed residue T29 (*CNF*29 CaM), which is distant from the putative CaM-NOS interface (**Figure 1**).

CNF was site-specifically introduced into CaM via amber suppression.³⁹ We first introduced *CNF* at V108 on helix E within the C-terminal lobe. Tandem mass spectrometry (MS/MS) of trypsin-digested protein (**Figure S2**) and intact protein MS (**Figure S6**) confirm the site-specific and efficient *CNF* incorporation at residue 108 of CaM. MS characterization of *CNF*29 CaM has also validated high-fidelity incorporation of *CNF* at residue 29 (**Figures S3 and S8**).

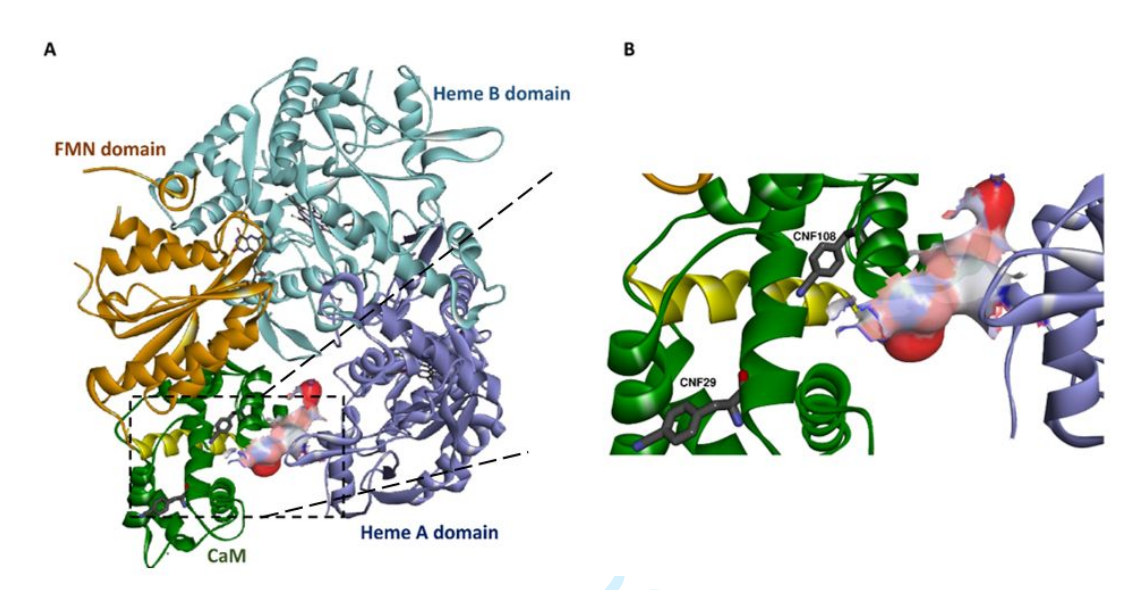


Figure 1. (A) Docking model of an oxyFMN construct of human iNOS.³⁷ The FMN subdomain (brown) docks onto the dimeric heme domain (cyan and purple), and CaM protein (green) binds to the linker (yellow) in between the FMN and heme A domains. The FMN subdomain docks onto the heme B domain in another subunit, allowing for intersubunit electron transfer between the FMN and heme centers. For clarity, the second FMN subdomain and CaM molecule are omitted. (B) Zoomed-in view of the *CNF* labeling sites relative to the CaM-heme(NOS) docking interface. *CNF* is inserted in CaM at residue 108 near an electrostatic patch (colored surface) in the interface, as a sensitive vibrational probe of CaM-heme(NOS) docking. *CNF*108 side chain does not clash with the docking interface residues. In another instance, a separate CaM protein is used as a control, where *CNF* is inserted at residue 29. This insertion site is far from the interface between CaM and NOS. The docking model is adapted from our previous work,³⁶ and the selected CaM

site (108 or 29) is mutated to unnatural amino acid *CNF* using UCSF Chimera and SwissSideChain rotamers.

The *CN*F-labeled CaM displays slightly different UV absorption spectra compared to the wild type (wt) CaM (**Figure S1**): the 280 nm shoulder is more obvious for *CN*F108 CaM. This is expected since the absorption spectrum of *CN*F itself has unique maxima at 233 and 280 nm.⁴⁰ The presence of *CN*F also increases the extinction co-efficient at 277 nm (**Table S1**). In general, the CaM protein retains its characteristic as a relatively low-absorption molecule in the mid-UV range.

We next examined the NO production activity by the *CNF*-labeled CaM-bound NOS enzyme. *CNF*108 CaM and *CNF*29 bound iNOS holoprotein exhibit similar NO production activity as the wt (**Table S2**). The *CNF*108 "mutation" has rather small effect on iNOS enzyme activation by CaM, as does the *CNF*29 variant. The *CNF* is thus a neutral spectroscopic sensor for monitoring the CaM-NOS interactions.

Due to instability in absence of CaM, iNOS holoprotein or oxyFMN was co-expressed with *CNF* CaM (see Supporting Information). We cloned the CaM gene into the same vector that contains the iNOS gene, to only have two plasmids transfected into the *E. coli* for *CNF* incorporation into the CaM protein co-expressed with iNOS. It is challenging to co-express a protein containing an unnatural amino acid along with a large protein such as iNOS. We optimized the *E. coli* strains and growth conditions, resulting in the successful production of milligram quantities of *CNF*-labeled CaM coexpressed with iNOS. This was achieved by using C321.ΔA, an *E. coli* strain designed for unnatural amino acid incorporation.⁴¹ MS/MS of trypsin-digested protein (**Figure S4** and S5) and intact protein MS (**Figure S7** and S9) confirmed the site-specific and efficient *CNF* incorporation at residues 108 and 29 of CaM when coexpressed with iNOS, respectively. These

MS results clearly illustrate that the *CN*F probe has been incorporated at the 108 or 29 site in the co-expressed CaM selectively and effectively.

A sample of the complex of CaM with the iNOS peptide was prepared by mixing CaM with the synthetic peptide. Given the K_D values (< 1 nM for p-iNOS),^{33, 42, 43} basically all the CaM should be bound to the iNOS peptide under the experimental conditions (the peptide and CaM are at μ M concentration levels and in 1:1 molar ratio). Additionally, binding of the iNOS peptide to the *CNF* CaM protein was verified by intact protein MS (**Figure S10**).

We next examined the protein samples via IR spectroscopy. The IR spectra of the *CNF*-labeled CaM alone exhibit absorption band(s) with frequencies in the range 2228–2236 cm⁻¹ as anticipated for the C=N vibration.^{30, 44, 45} For *CNF*29 CaM, a single absorption band appears at 2235.8 cm⁻¹ (**Figure S13**). This relatively high frequency is the same as observed for the free *CNF* amino acid in aqueous solution, consistent with the location of the residue at the solvent-exposed surface of CaM. Corroborating this interpretation, the frequency decreases with heating (**Figure S15**). C=N frequencies primarily vary from electrostatic interactions (i.e. a Stark shift) or to hydrogen bonding. Of these, hydrogen bonding interactions are more sensitive to temperature, so analysis of the temperature dependence of the CN frequency is helpful to discriminate these mechanisms.⁴⁶ The observed downshift in frequency of *CNF*29 with temperature is consistent with disruption of *CNF*29-water hydrogen bonding.

Upon binding to holoprotein or oxyFMN iNOS, the spectra of *CN*F29 CaM are essentially unchanged, compared to the individual CaM protein (**Figure 2, Table S4**). The insensitivity to its association with the iNOS protein is anticipated given the location (**Figure 1**), designed to be distant from the regions of interaction with iNOS. In contrast, the IR spectrum of *CN*F108 CaM is highly sensitive to association with iNOS protein. All IR spectra for *CN*F108 CaM are best

modeled as a superposition of two bands, indicating population of two major distinct states (Figure 2, **Table S4**). Additional details and figures to illustrate spectral processing and analysis are provided in Supporting Information (**Figures S11-S14**). The frequencies of the bands (~ 2229 and 2234 cm⁻¹) are essentially constant among all samples (*CN*F108 CaM alone, *CN*F108 CaM in complexation with iNOS peptide, iNOS oxyFMN construct or full-length iNOS). However, variation is found in the relative areas and linewidths.

For individual *CN*F108 CaM, the two bands are nearly equal in area (48% and 52%), indicating *CN*F108 populates two states in CaM about equally (**Figure 2**; **Table S4**). In contrast to *CN*F29, the temperature-induced changes in the spectra do not support the C≡N group of *CN*F108 participating in hydrogen bonding. Upon increase in temperature, the spectrum upshifts and narrows, eventually appearing as a single band (**Figure S16**). Modeling indicates that the lower frequency band upshifts, whereas the higher frequency band remains at about the same frequency but disappears with a transition midpoint around 55°C.

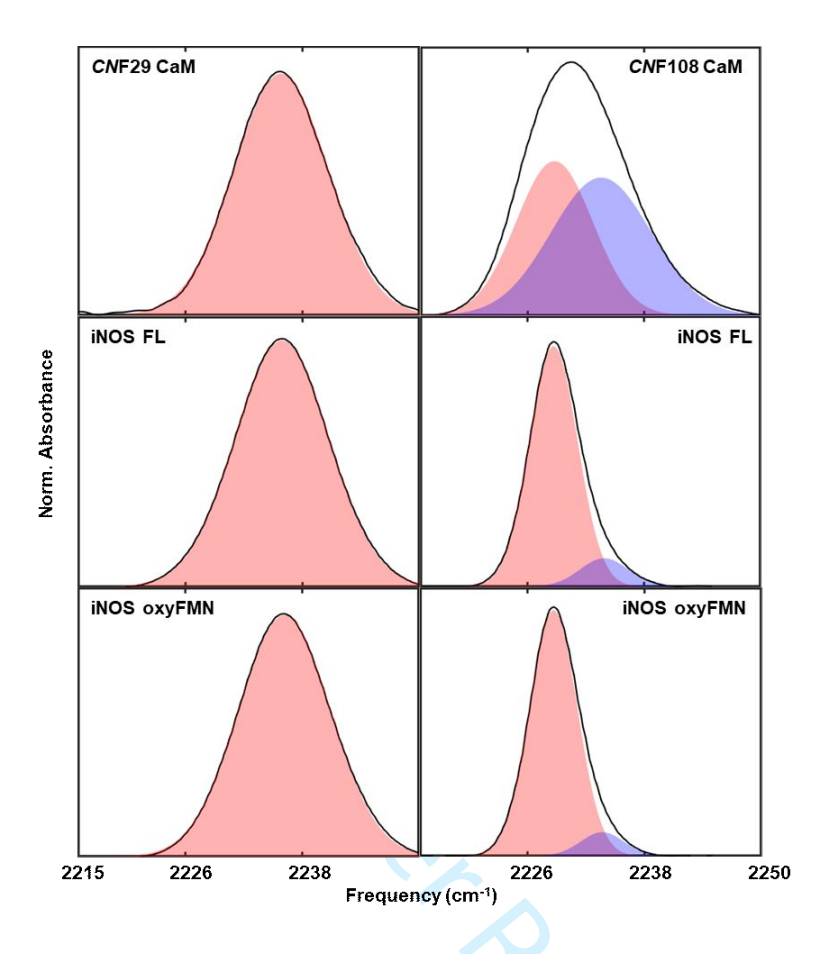


Figure 2. FT IR spectra of *CN*F29 (left panel) and *CN*F108 (right panel) CaM alone (top row) or associated with full-length (FL) iNOS (middle row) or the oxyFMN construct (bottom row).

Upon association of CNF108 CaM with iNOS holoprotein, the absorption envelope shifts toward lower frequency. The band at lower frequency (2229 cm⁻¹) dominates the spectrum (~90% relative area) (**Figure 2**). In the complex of CNF108 CaM with iNOS the linewidths are also significantly (~40%) narrower than CNF108 CaM alone (**Table S4**). This narrowing suggests the $C\equiv N$ probe experiences a more limited distribution of environments, consistent with the side chain being more constricted when CaM is bound to iNOS. Additionally, the observation of a dominant IR band suggests a rather homogeneous environment when CaM is associated with iNOS, even though two copies of CaM are presumed present per dimer enzyme. This implies that the CaM proteins adopt the same conformation at CNF108 in complexation with the two subunits of iNOS.

The spectrum of *CN*F108 CaM was then characterized when associated with the oxyFMN construct or the iNOS peptide (**Figure 2 and Figure S13**). The IR spectra of *CN*F108 are nearly the same when the *CN*F108 CaM is bound to the full-length NOS proteins, the oxyFMN, or the peptide. This indicates that the binding-induced change at *CN*F108, as observed in the FT IR spectra, is primarily attributed to interaction with the canonical CaM recognition sequence. We cannot make any structural conclusions about the direction of IR frequency shift upon iNOS protein or peptide complexation with a specific type of molecular interactions between the CNF probe and iNOS molecule. These shifts in 1D IR provide only qualitative information but do show that the labeled CaM 108 site is likely interacting with NOS.

To better understand the environment of the C≡N probe, we performed molecular dynamics (MD) simulations for *CN*F108 in CaM in complexation with the iNOS peptide (**Figure 3**) (see Supporting Information for details). Consistent with the temperature-dependent IR analysis, the simulations do not indicate appreciable hydrogen bonding by *CN*F108 in the complex with the peptide (**Table S5**). We were unable to identify an order parameter with a bimodal distribution that would account for the two distinct absorptions observed experimentally. However, MD simulations with extensive sampling of Ca²+-loaded CaM in absence of its target/ligand have captured multiple distinct minima in the energy landscape associated with interhelical motions within and between EF hands of a lobe. ⁴⁷⁻⁴⁹ Interhelical displacements likewise differentiate the average structures from our MD simulations of the complexes with p-iNOS and influence the packing of the C≡N probe and nearby hydrophobic side chains (**Figure S19**, **Table S6**). This initial interpretation points to the recognition of NOS isoforms by CaM being differentiated by interhelical motions within the C-lobe, although more extensive sampling is needed to observe the conformational heterogeneity underlying the IR bands.

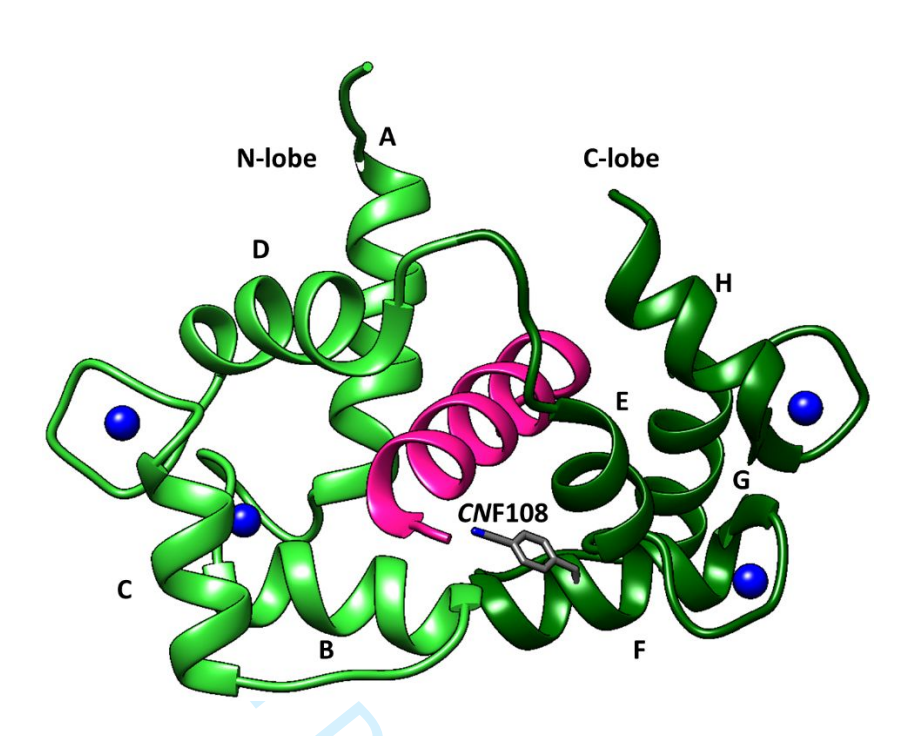


Figure 3. Ribbon model of the average structure of the *CN*F108 CaM (green) in complex with p-iNOS (pink). The side chain of *CN*F108 is shown in purple in stick representation, and Ca²⁺ ions are shown as blue spheres.

In summary, we demonstrate that site-specific labeling with frequency-resolved vibrational probes is a unique approach to probe local conformational heterogeneity involved in CaM interactions with the iNOS isoform. Additionally, we wish to emphasize that selective incorporation of CNF, an unnatural amino acid, into CaM co-expressed with the large iNOS protein is a challenging endeavor. We have refined the methodologies for both site-specific CNF incorporation and the quantification of CNF% within the CaM-iNOS complex. These have the potential to benefit research in other protein-protein complexes.

Introduction of the *CNF* probe at additional locations in CaM and the NOS isoforms is ongoing to further map out the contacts and interfaces between the CaM and (sub)domains of the NOS isoforms. This will help to better elucidate how the conformational ensembles differentially

contribute to the regulation of NOS activity. Understanding these mechanistical differences may bolster efforts to selectively target NOS isoforms for therapeutic intervention. Further studies of the labeled proteins by 2D IR spectroscopy, which is resolved in both the frequency and time domains, is also ongoing. These studies provide additional valuable information regarding local probe frequency heterogeneity such as that seen in Fig. 2. For example, they can provide a more rigorous estimation of the relative populations of the underlying states and whether they Illy (< 5 ps) or ... interconvert rapidly (< 5 ps) or slowly (> 5 ps).

Supporting Information

Protein expression and purification, LC–MS/MS analysis, NOS enzymatic activity assay, mass spectroscopy, IR sample preparation, FT IR measurements and analysis, MD simulations details and analysis (Figures S1–S19 and Tables S1–S7)

Accession Codes Human iNOS, P35228

Funding Sources

This material is based upon work funded by NIH GM133973 and NSF 2041692 (C.F.) and NIH GM148290 and DESC0018983 (M.C.T.). This work was also supported in part by NIH P20GM130422 and P30ES032755.

Acknowledgement

We thank Dr. Henning Tidow for sharing the pET28aCaMC3His plasmid. Computational aspects of this research were supported in part by Lilly Endowment, Inc., through its support for the Indiana University Pervasive Technology Institute.

References

- (1) Moncada, S.; Higgs, E. A. The discovery of nitric oxide and its role in vascular biology. *Br J Pharmacol* **2006**, *147*, 193-201. DOI: 10.1038/sj.bjp.0706458 From NLM Medline.
- (2) Akanji, M. A.; Adeyanju, A. A.; Rotimi, D.; Adeyemi, O. S. Nitric Oxide Balance in Health and Diseases: Implications for New Treatment Strategies. *The Open Biochemistry Journal* **2020**, *14*(1), 25-32. DOI: 10.2174/1874091x02014010025.
- (3) Lundberg, J. O.; Weitzberg, E. Nitric oxide signaling in health and disease. *Cell* 2022, 185(16), 2853-2878. DOI: 10.1016/j.cell.2022.06.010 From NLM Medline.
- (4) Mourad, M.; Aly, O.; Mourad, A. Nitric oxide: Synthesis, Pathophysiology and Application on Oncology and Cardiovascular Diseases. *Octahedron Drug Research* **2022**, *1*, 34-49. DOI: 10.21608/odr.2022.154048.1001.
- (5) Lancaster, J. R., Jr.; Xie, K. Tumors face NO problems? *Cancer Res* 2006, 66 (13), 6459-6462.DOI: 10.1158/0008-5472.CAN-05-2900 From NLM Medline.
- (6) Forstermann, U.; Sessa, W. C. Nitric oxide synthases: regulation and function. *Eur Heart J* **2012**, *33* (7), 829-837, 837a-837d. DOI: 10.1093/eurheartj/ehr304 From NLM Medline.

- (7) Gantner, B. N.; LaFond, K. M.; Bonini, M. G. Nitric oxide in cellular adaptation and disease.
 Redox Biol 2020, 34, 101550-101561. DOI: 10.1016/j.redox.2020.101550 From NLM Medline.
- (8) Kurkin, D. V.; Abrosimova, E. E.; Bakulin, D. A.; Kovalev, N. S.; Dubrovina, M. A.; Borisov,
- A. V.; Strygin, A. V.; Morkovin, E. I.; Tyurenkov, I. N. Activity Modulation of Various Nitric

Oxide Syntases as an Approach to Endothelial Dysfunction Therapy. Pharmacy & Pharmacology

, 10(2), 130-153. DOI: 10.19163/2307-9266-2022-10-2-130-153.

- (9) Soundararajan, L.; Dharmarajan, A.; Samji, P. Regulation of pleiotropic physiological roles of nitric oxide signaling. *Cellular Signalling* 2023, *101*, 110496. DOI: https://doi.org/10.1016/j.cellsig.2022.110496.
- (10) Roman, L. J.; Marta'sek, P.; Masters, B. S. S. Intrinsic and Extrinsic Modulation of Nitric Oxide Synthase Activity. *Chem. Rev.* **2002**, *102*, 1179–1189. DOI: 10.1021/cr000661e.
- (11) Li, H.; Poulos, T. L. Structure-function studies on nitric oxide synthases. *J Inorg Biochem* **2005**, *99*(1), 293-305. DOI: 10.1016/j.jinorgbio.2004.10.016 From NLM Medline.
- (12) Daff, S. NO synthase Structures and mechanisms. *Nitric Oxide* **2010**, *23*, 1-11. DOI: 10.1016/j.niox.2010.03.001.

- (13) Leferink, N. G.; Hay, S.; Rigby, S. E.; Scrutton, N. S. Towards the free energy landscape for catalysis in mammalian nitric oxide synthases. *FEBS J* **2015**, *282* (16), 3016-3029. DOI: 10.1111/febs.13171 From NLM Medline.
- (14) Campbell, M. G.; Smith, B. C.; Potter, C. S.; Carragher, B.; Marletta, M. A. Molecular architecture of mammalian nitric oxide synthases. *Proc Natl Acad Sci U S A* **2014**, *111* (35), E3614-3623. DOI: 10.1073/pnas.1413763111 From NLM Medline.
- (15) Volkmann, N.; Martasek, P.; Roman, L. J.; Xu, X. P.; Page, C.; Swift, M.; Hanein, D.; Masters, B. S. Holoenzyme structures of endothelial nitric oxide synthase an allosteric role for calmodulin in pivoting the FMN domain for electron transfer. *J Struct Biol* **2014**, *188* (1), 46-54. DOI: 10.1016/j.jsb.2014.08.006 From NLM Medline.
- (16) Yokom, A. L.; Morishima, Y.; Lau, M.; Su, M.; Glukhova, A.; Osawa, Y.; Southworth, D. R. Architecture of the nitric-oxide synthase holoenzyme reveals large conformational changes and a calmodulin-driven release of the FMN domain. *J Biol Chem* **2014**, *289* (24), 16855-16865. DOI: 10.1074/jbc.M114.564005 From NLM Medline.

- (17) Arnett, D. C.; Bailey, S. K.; Johnso, C. K. Exploring the conformations of nitric oxide synthase with fluorescence. *Frontiers In Bioscience, Landmark,* **2018**, *23*, 2133-2145. DOI: 10.2741/4694.
- (18) Li, J.; Zheng, H.; Feng, C. Deciphering mechanism of conformationally controlled electron transfer in nitric oxide synthases. *Frontiers In Bioscience, Landmark*, **2018**, *23*, 1803-1821. DOI: 10.2741/4674.
- (19) Astashkin, A. V.; Li, J.; Zheng, H.; Feng, C. Positional Distributions of the Tethered Modules in Nitric Oxide Synthase: Monte Carlo Calculations and Pulsed EPR Measurements. *J Phys Chem A* **2019**, *123* (32), 7075-7086. DOI: 10.1021/acs.jpca.9b05388 From NLM Medline.
- (20) Bignon, E.; Rizza, S.; Filomeni, G.; Papaleo, E. Use of Computational Biochemistry for Elucidating Molecular Mechanisms of Nitric Oxide Synthase. *Comput Struct Biotechnol J* **2019**, *17*, 415-429. DOI: 10.1016/j.csbj.2019.03.011 From NLM PubMed-not-MEDLINE.
- (21) Sessa, W. C.; Harrison, J. K.; Barber, C. M.; Zeng, D.; Durieux, M. E.; D'Angelo, D. D.; Lynch, K. R.; Peach, M. J. Molecular cloning and expression of a cDNA encoding endothelial cell nitric oxide synthase. *Journal of Biological Chemistry* **1992**, *267* (22), 15274-15276. DOI: 10.1016/s0021-9258(19)49528-8.

- (22) Ruan, J.; Xie, Q.; Hutchinson, N.; Cho, H.; Wolfe, G. C.; Nathan, C. Inducible nitric oxide synthase requires both the canonical calmodulin-binding domain and additional sequences in order to bind calmodulin and produce nitric oxide in the absence of free Ca2+. *J Biol Chem* **1996**, *271* (37), 22679-22686. DOI: 10.1074/jbc.271.37.22679 From NLM Medline.
- (23) Tejero, J.; Hannibal, L.; Mustovich, A.; Stuehr, D. J. Surface charges and regulation of FMN to heme electron transfer in nitric-oxide synthase. *J Biol Chem* **2010**, *285* (35), 27232-27240. DOI: 10.1074/jbc.M110.138842 From NLM Medline.
- (24) Li, W.; Chen, L.; Lu, C.; Elmore, B. O.; Astashkin, A. V.; Rousseau, D. L.; Yeh, S. R.; Feng, C. Regulatory role of Glu546 in flavin mononucleotide-heme electron transfer in human inducible nitric oxide synthase. *Inorg Chem* **2013**, *52*(9), 4795-4801. DOI: 10.1021/ic3020892 From NLM Medline.
- (25) Haque, M. M.; Tejero, J.; Bayachou, M.; Kenney, C. T.; Stuehr, D. J. A cross-domain charge interaction governs the activity of NO synthase. *J Biol Chem* **2018**, *293* (12), 4545-4554. DOI: 10.1074/jbc.RA117.000635 From NLM Medline.

(26) Li, J.; Zheng, H.; Wang, W.; Miao, Y.; Sheng, Y.; Feng, C. Role of an isoform-specific residue at the calmodulin-heme (NO synthase) interface in the FMN - heme electron transfer. *FEBS Lett* **2018**, *592* (14), 2425-2431. DOI: 10.1002/1873-3468.13158 From NLM Medline.

(27) Haque, M. M.; Bayachou, M.; Tejero, J.; Kenney, C. T.; Pearl, N. M.; Im, S. C.; Waskell, L.; Stuehr, D. J. Distinct conformational behaviors of four mammalian dual-flavin reductases (cytochrome P450 reductase, methionine synthase reductase, neuronal nitric oxide synthase, endothelial nitric oxide synthase) determine their unique catalytic profiles. *FEBS J*2014, *281* (23), 5325-5340. DOI: 10.1111/febs.13073 From NLM Medline.

- (28) Hedison, T. M.; Hay, S.; Scrutton, N. S. A perspective on conformational control of electron transfer in nitric oxide synthases. *Nitric Oxide* **2017**, *63*, 61-67. DOI: 10.1016/j.niox.2016.09.002 From NLM Medline.
- (29) Hanson, Q. M.; Carley, J. R.; Gilbreath, T. J.; Smith, B. C.; Underbakke, E. S. Calmodulin-induced Conformational Control and Allostery Underlying Neuronal Nitric Oxide Synthase Activation. *J Mol Biol* **2018**, *430* (7), 935-947. DOI: 10.1016/j.jmb.2018.02.003 From NLM Medline.

- (30) Tucker, M. J.; Oyola, R.; Gai, F. A novel fluorescent probe for protein binding and folding studies: p-cyano-phenylalanine. *Biopolymers* **2006**, *83* (6), 571-576. DOI: 10.1002/bip.20587 From NLM Medline.
- (31) Creon, A.; Josts, I.; Niebling, S.; Huse, N.; Tidow, H. Conformation-specific detection of calmodulin binding using the unnatural amino acid p-azido-phenylalanine (AzF) as an IR-sensor. *Struct Dyn* **2018**, *5* (6), 064701-064712. DOI: 10.1063/1.5053466 From NLM PubMed-not-MEDLINE.
- (32) Zhang, J.; Wang, L.; Zhang, J.; Zhu, J.; Pan, X.; Cui, Z.; Wang, J.; Fang, W.; Li, Y. Identifying and Modulating Accidental Fermi Resonance: 2D IR and DFT Study of 4-Azido-l-phenylalanine. *J Phys Chem B* 2018, *122* (34), 8122-8133. DOI: 10.1021/acs.jpcb.8b03887 From NLM Medline. (33) Venema, R. C.; Sayegh, H. S.; Kent, J. D.; Harrison, D. G. Identification, Characterization, and Comparison of the Calmodulin-binding Domains of the Endothelial and Inducible Nitric Oxide Synthases. *THE JOURNAL OF BIOLOGICAL CHEMISTRY* 1996, *271* (11), 6435–6440. DOI: 10.1074/jbc.271.11.6435.
- (34) Ghosh, D. K.; Holliday, M. A.; Thomas, C.; Weinberg, J. B.; Smith, S. M.; Salerno, J. C. Nitric-oxide synthase output state. Design and properties of nitric-oxide synthase oxygenase/FMN

domain constructs. *J Biol Chem* **2006**, *281* (20), 14173-14183. DOI: 10.1074/jbc.M509937200 From NLM Medline.

- (35) Li, J.; Zheng, H.; Wang, W.; Miao, Y.; Sheng, Y.; Feng, C. Role of an isoform-specific residue at the calmodulin-heme(NO synthase) interface in the FMN heme electron transfer. *FEBS Lett.* **2018**, *592*, 2425-2431. DOI: 10.1002/1873-3468.13158.
- (36) Sheng, Y.; Zhong, L.; Guo, D.; Lau, G.; Feng, C. Insight into structural rearrangements and interdomain interactions related to electron transfer between flavin mononucleotide and heme in nitric oxide synthase: A molecular dynamics study. *J Inorg Biochem* **2015**, *153*, 186-196. DOI: 10.1016/j.jinorgbio.2015.08.006 From NLM Medline.
- (37) Hollingsworth, S. A.; Holden, J. K.; Li, H.; Poulos, T. L. Elucidating nitric oxide synthase domain interactions by molecular dynamics. *Protein Sci* **2016**, *25* (2), 374-382. DOI: 10.1002/pro.2824 From NLM Medline.
- (38) Smith, B. C.; Underbakke, E. S.; Kulp, D. W.; Schief, W. R.; Marletta, M. A. Nitric oxide synthase domain interfaces regulate electron transfer and calmodulin activation. *Proc Natl Acad Sci U S A* 2013, *110* (38), E3577-3586. DOI: 10.1073/pnas.1313331110 From NLM Medline.

- (39) Schultz, K. C.; Supekova, L.; Ryu, Y.; Xie, J.; Perera, R.; Schultz, P. G. A Genetically Encoded Infrared Probe. *JACS* **2006**, *128*, 13984-13985. DOI: https://doi.org/10.1021/ja0636690. (40) Matthew J. Tucker; Rolando Oyola; Ga, F. Conformational Distribution of a 14-Residue Peptide in Solution A FluorescenceResonance Energy Transfer Study. *J. Phys. Chem. B* **2005**, *109*, 4788-4795. DOI: https://doi.org/10.1021/jp044347q.
- (41) Pirman, N. L.; Barber, K. W.; Aerni, H. R.; Ma, N. J.; Haimovich, A. D.; Rogulina, S.; Isaacs, F. J.; Rinehart, J. A flexible codon in genomically recoded Escherichia coli permits programmable protein phosphorylation. *Nat Commun* **2015**, *6*, 8130. DOI: 10.1038/ncomms9130 From NLM Medline.
- (42) Zhang, M.; Vogel, H. J. Characterization of the calmodulin-binding domain of rat cerebellar nitric oxide synthase. *Journal of Biological Chemistry* **1994**, *269* (2), 981-985. DOI: 10.1016/s0021-9258(17)42208-3.
- (43) Yuan, T.; Vogel, H. J.; Sutherland, C.; Walsh, M. P. Characterization of the Ca2+ -dependent and -independent interactions between calmodulin and its binding domain of inducible nitric oxide synthase. *FEBS Lett* **1998**, *431* (2), 210-214. DOI: 10.1016/s0014-5793(98)00750-9 From NLM Medline.

- (44) Horness, R. E.; Basom, E. J.; Thielges, M. C. Site-selective Characterization of Src Homology 3 Domain Molecular Recognition with Cyanophenylalanine Infrared Probes. *Anal Methods* **2015**, 7, 7234-7241. DOI: 10.1039/C5AY00523J From NLM Publisher.
- (45) Basom, E. J.; Maj, M.; Cho, M.; Thielges, M. C. Site-Specific Characterization of Cytochrome P450cam Conformations by Infrared Spectroscopy. *Anal Chem* **2016**, *88* (12), 6598-6606. DOI: 10.1021/acs.analchem.6b01520 From NLM Medline.
- (46) Adhikary, R.; Zimmermann, J.; Dawson, P. E.; Romesberg, F. E. Temperature Dependence of CN and SCN IR Absorptions Facilitates Their Interpretation and Use as Probes of Proteins.

 Anal Chem 2015, 87 (22), 11561-11567. DOI: 10.1021/acs.analchem.5b03437 From NLM Medline.
- (47) Gsponer, J.; Christodoulou, J.; Cavalli, A.; Bui, J. M.; Richter, B.; Dobson, C. M.; Vendruscolo, M. A coupled equilibrium shift mechanism in calmodulin-mediated signal transduction. *Structure* **2008**, *16* (5), 736-746. DOI: 10.1016/j.str.2008.02.017 From NLM Medline.
- (48) Shukla, D.; Peck, A.; Pande, V. S. Conformational heterogeneity of the calmodulin binding interface. *Nat Commun* **2016**, *7*, 10910. DOI: 10.1038/ncomms10910 From NLM Medline.

(49) Kawasaki, H.; Soma, N.; Kretsinger, R. H. Molecular Dynamics Study of the Changes in Conformation of Calmodulin with Calcium Binding and/or Target Recognition. *Sci Rep* 2019, 9
(1), 10688. DOI: 10.1038/s41598-019-47063-1 From NLM Medline.



Supporting Information

Probing Calmodulin-NO Synthase Interactions via Site-Specific Infrared Spectroscopy: An Introductory Investigation

Swapnil Singh ^{‡a}, Yadav Prasad Gyawali^{‡b}, Ting Jiang^b, Gregory S Bukowski ^a, Huayu Zheng^b, Haikun Zhang^b, Rebecca Owopetu^b, Megan C Thielges *a, Changjian Feng *b

^a Department of Chemistry, Indiana University, Bloomington, Indiana 47405, United States ^b College of Pharmacy, University of New Mexico, Albuquerque, New Mexico 87131, United States

*Corresponding Authors: efeng@unm.edu, thielges@indiana.edu

Table of Contents

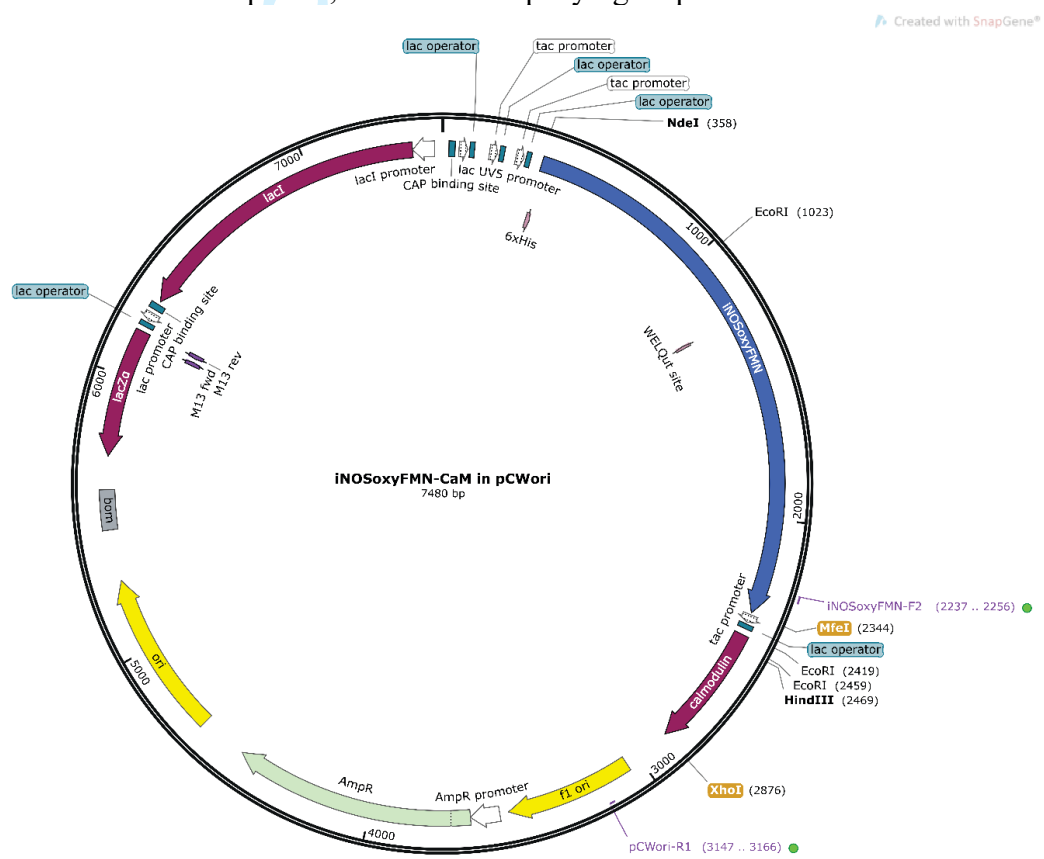
| 1. Construction of CNF29 CaM plasmid | |
|--|-----|
| 2. Construction of iNOS-CNF CaM plasmids | S3 |
| 3. Overexpression and purification of CNF108 CaM and CNF29 CaM | S4 |
| 4. Overexpression and purification of CNF108 CaM- and CNF29 CaM-bound iNOS | S4 |
| 5. UV-Visible spectroscopy of CNF CaM | S4 |
| 6. NOS enzymatic activity assay | S5 |
| 7. LC-MS/MS of <i>CN</i> F CaM | S5 |
| 8. Mass spectrometry (MS) of intact CNF CaM | S6 |
| 9. CNF108 CaM-peptide binding validated by native intact protein MS | |
| 10. Sample preparation for infrared spectroscopy | |
| 11. Infrared spectroscopy measurements and analyses | S7 |
| 12. Molecular dynamics simulations | S9 |
| 13. Figures and Tables | S11 |
| References | S26 |

1. Construction of CNF29 CaM plasmid

Overall, a tRNA charged with the 4-cyano-L-phneylalaine (*CNF*) is engineered to recognize an amber TAG stop codon, which allows for incorporation of *CNF* in the growing polypeptide chain via nonsense codon suppression.¹ The wild type pET28aCaMC3His plasmid was shared by Dr. Henning Tidow in which the *Xenopus laevis* CaM sequence was cloned into a modified pET28a vector containing a C-terminal His₆ tag. The V108TAG variant plasmid was also provided by Dr. Tidow. For incorporation of *CNF* at T29 site, an amber stop codon was introduced by QuikChange site-directed mutagenesis into the CaM sequence. TAG codon installation at 29 was verified by DNA sequencing.

2. Construction of iNOS-CNF CaM plasmids

The p209 CaM sequence was cloned into a pCWori plasmid that contains the N-terminal His6 tagged human iNOS sequence (oxyFMN or full length).² The CaM sequence was cloned downstream of the iNOS sequence; see the accompanying map below.



The combined overlap extension PCR (COE-PCR)³ was performed and the PCR fragments were assembled in the pCWori vector using NEBuilder HiFi DNA assembly cloning kit (New England Biolabs Inc.). The primers for constructing the TAG CaM variant plasmid are listed in the accompanying Table. The assembly including the TAG mutant in CaM was confirmed by sequencing the plasmid (Genewiz).

Page 30 of 53

| Plasmid | Primer | Primer sequence (5' to 3') |
|---------------------------|--------------------------|---|
| T29TAG | iNOS FL-Mfel-CaM-Forward | GATGTCAGCGCTCTGAGGACAATTGTTGACAATTAATCATCGGCTCG |
| CaM·iNOS full length | T29TAG P209 CaM-Reverse | TGTGATTGTGCCATCGCCGTCCTTGTCGAAC |
| (FL) | T29TAG P209 CaM-Forward | GGCGATGGCACAATCACATAGAAGGAGCTGGGGAC |
| | iNOS-Xhol-CaM-Reverse | GCTCATGTTTGACAGCTTATCATCGATACTCGAGTCACTTAGCCGTCATCATTTG |
| V108TAG CaM·iNOS FL | iNOS FL-Mfel-CaM-Forward | GATGTCAGCGCTCTGAGGACAATTGTTGACAATTAATCATCGGCTCG |
| | P209 CaM-Reverse | GTGACGTAGCTCAGCAGCGCTGATGTAGCCGTT |
| | V108TAG P209 CaM-Forward | GCGCTGCTGAGCTACGTCACTAGATGACGAATCTCGG |
| | iNOS-Xhol-CaM-Reverse | GCTCATGTTTGACAGCTTATCATCGATACTCGAGTCACTTAGCCGTCATCATTTG |

3. Overexpression and purification of CNF108 CaM and CNF29 CaM

The pET28a CaM TAG variant plasmid and pULTRA-CNF (Addgene #48215) were cotransformed via electroporation into BL21(DE3) cells (Intact Genomics Cat. No. 1252-24). The cells were grown in TB media at 37 °C, supplemented with 25 μg/ml kanamycin and 25 μg/ml streptomycin. Protein expression was induced at OD₆₀₀ = 0.6 – 0.8 by addition of a final concentration of 1 mM IPTG, and 1 mM CNF. The cells were harvested after 4 hours and stored at -80 °C. The cell pellets were resuspended in a pH 7.5 buffer containing 50 mM MOPS, 100 mM KCl, 1 mM EDTA, 1 mM dithiothreitol (DTT), 0.5 mg/mL lysozyme and complete protease inhibitor cocktail. The cells were then lysed by pulsed sonication in ice. The purification of CNF labelled CaM was performed using previous procedure. CaM concentration was determined using an extinction coefficient of 3029 M⁻¹ cm⁻¹ at 277 nm (see SI section 5). The purity of isolated CNF-CaM protein was assessed by SDS-PAGE, and its UV-vis spectrum was similar to wild type CaM (Figure S1).

4. Overexpression and purification of CNF108 CaM- and CNF29 CaM-bound iNOS

The pULTRA-CNF plasmid (Addgene #48215) and the iNOS-CaM plasmid containing the TAG variant were co-transformed via heat shock (42 °C, 30 seconds) into a C321. Δ A strain designed to facilitate unnatural amino acid incorporation.⁵ The cells were grown in TB media at 30°C, supplemented with 100 µg/ml ampicillin and 25 µg/ml streptomycin. Protein expression was induced at OD600 = 0.8-1.0 by addition of a final concentration of 0.5 mM IPTG and supplemented with 1 mM CNF, 0.4 mM delta-aminolevulinic acid (δ -ALA, a heme precursor) and a pinch of riboflavin, and then grown at 25°C for 40 h. The cells were harvested and stored at - 80 °C. The protein was purified using the published procedure.² The iNOS holoprotein was intact and functional, based on the SDS PAGE and NO production activity data.

5. UV-Visible spectroscopy of CNF CaM

UV-visible spectra of *CNF*-labeled CaM were measured in 50 mM Tris-Cl buffer, pH 7.5, containing 1 mM CaCl₂ (Figure S1). The concentrations of the same protein samples were determined in at least triplicate using a Pierce 660nm Protein Assay Kit (Thermo Scientific). The

extinction coefficient at 277 nm was then calculated from the observed UV-visible absorbance and the protein concentration measured from Pierce assay (Table S1).

6. NOS enzymatic activity assay

Steady-state rate of NO production by human iNOS holoprotein was determined in 50 mM Tris, pH 7.4, 100 mM NaCl, 5 μM 6R-5,6,7,8-tetrahydrobiopterin (H₄B), and 200 μM CaCl₂.⁶ Assay solutions contained 100 μM L-Arg, 100 μM NADPH, and 8 μM oxyhemoglobin. The NADPH solution was made freshly on the date of experiments. Reaction was initiated by adding the iNOS protein (20 nM final concentration), and rate of NO synthesis was determined using an extinction coefficient of 60 mM⁻¹ cm⁻¹ at 401 nm (Table S2).

7. LC-MS/MS of CNF CaM

The LC-MS/MS analysis was performed to verify the site-specific incorporation of CNF into the CaM protein. Gel bands of CaM were excised, disulfide bonds were reduced with DTT, and free cysteines were alkylated with iodoacetamide prior to the digestion in 50 mM ammonium bicarbonate pH 8.5 with 20 ng/microliter trypsin/lysine C (Promega Corporation, Madison, WI) overnight at 37 °C. LC-MS/MS analysis was conducted on a Q Exactive Classic mass spectrometer (Thermo Fisher Scientific, San Jose, CA) equipped with an Easy Spray nanoESI source. The peptides were eluted from an Acclaim Pepmap 100 trap column (75 micron ID × 2 cm, Thermo Scientific) onto an Acclaim PepMap RSLC analytical column (75 micron ID × 15 cm, Thermo Scientific) using a 2-50% gradient of solution B (acetonitrile, 0.1% formic acid) over 55 minutes, 50-95% solution B over 5 minutes, 95% hold of solution B for 10 minutes, and finally a return to 2% solution B in 3 minute and another 7 minute hold of 2% solvent B. Solution A consisted of water and 0.1% formic acid. All flow rates were 300 nL/min using a Dionex Ultimate 3000 RSLCnano System (Thermo Scientific). Data dependent scanning was performed by the Xcalibur software using a survey scan at 70,000 resolution, scanning mass/charge (m/z) 375-2000, automatic gain control (AGC) target of 3e6 and a maximum injection time (IT) of 100 ms, followed by higher-energy collisional dissociation (HCD) tandem mass spectrometry (MS/MS) at 30 normalized collision energy (nce) of the 10 most intense ions at a resolution of 17,500, an isolation width of 1.5 m/z, an AGC of 1e5 and a maximum IT of 60 milliseconds. Dynamic exclusion was set to place any selected m/z on an exclusion list for 20 seconds after a single MS/MS. Ions of charge state +1, 7, 8, >8 and unassigned were excluded from MS/MS, so were isotopes.

Tandem mass spectra were searched against a recombinant human CaM sequence, the Uniprot *E. coli* protein database and an additional common contaminant protein database (e.g., trypsin, keratins) obtained at ftp://ftp.thegpm.org/fasta/cRAP. All MS/MS spectra were searched using Thermo Proteome Discoverer v 2.5 (Thermo Fisher Scientific) considering fully tryptic peptides with up to 2 missed cleavage sites. Variable modifications considered during the search included cyano (24.9952 Da), methionine oxidation (15.995 Da), and cysteine carbamidomethylation (57.021 Da). Proteins were identified at 99% confidence with XCorr score cut-offs⁸ as determined by a reversed database search. The protein and peptide identification results were also visualized with Scaffold Q+S v 4.11 (Proteome Software Inc., Portland OR), a program that relies on various search engine results (i.e., Sequest, X!Tandem, MASCOT) and uses Bayesian statistics to reliably identify more mass spectra.⁹ Protein identifications were accepted that passed a minimum of two

peptides identified at 0.1% peptide False Discovery Rate and 90-99.9% protein confidence by the Protein Profit algorithm within Scaffold.

8. Mass spectrometry of intact CNF CaM protein

The intact protein MS analysis was conducted to measure the CNF incorporation efficiency, giving that the single amino acid difference does not affect the ionization efficiency of the protein. CaM, a rather small sized protein, is amendable to intact protein MS analysis. The isolated CNF108 CaM or CNF29 CaM itself was directly used for such analysis. For the co-expressed CNF CaM, the protein was dissociated from the bound CaM-iNOS complex prior to the intact protein MS analysis, which can be realized by gentle treatment of the protein with TFA in organic solvent. 15 μ L 100 μ M CNF108 CaM.iNOS protein or CNF29 CaM.iNOS was mixed with 35 μ L 0.1 % TFA in 50% ACN, and the sample was kept at room temperature for 20 minutes. The final CNF CaM protein concentration was 30 μ M in 35% ACN and 0.07% TFA. The solution was then subjected to UPLC-MS.

The intact mass of denatured CaM protein was determined by UPLC-MS. Desalting and LC separation was carried out on a Vanquish Flex Binary UHPLC (Thermo Fisher Scientific, San Jose, CA) using a Biobasic 4 column (5 μm; 50 x 2.1 mm; Thermo Fisher Scientific, San Jose, CA). Proteins were eluted using mobile phase A of 0.1% formic acid in water, mobile phase B of 0.1% formic acid in acetonitrile, and a 10 min gradient of 1) 3%-97% B over 6.5 min, 2) then a hold of B for 1.5 min, 3) return to A in 0.5 min, and 4) a final hold of A for 1.5 min. Eluted proteins were directly introduced to a Q-Exactive Orbitrap Classic mass spectrometer (Thermo Fisher Scientific, San Jose, CA) equipped with a HESI source (Thermo Fisher Scientific, San Jose, CA). Data acquisition was performed with a mass resolution of 70k, an AGC target of 3e6, a maximum IT of 200 ms and a scan range of 800-2000 m/z. For data analysis, intact protein masses were deconvoluted using FreeStyleTM 1.8 SP2 (Thermo Fisher Scientific, San Jose, CA).

9. CNF108 CaM-NOS peptide binding validated by native intact protein MS

The native protein MS was done to assess the CNF108 CaM-binding with the iNOS peptide (p-iNOS). The CNF108 CaM protein was buffer exchanged into ammonium acetate, a MS-compatible buffer, using an Amicon® Ultra 0.5 mL Centrifugal Filter with a regenerated cellulose membrane and a 10 kDa MWCO (Millipore, Billerica, Massachusetts, USA). 5 μ L of protein (4.8 mM in Tris storage buffer) was diluted with 450 μ L of 20 mM ammonium acetate, pH 7.0, and centrifuged at 14000 RPM for 20 min at 4 °C. The recovered sample after three cycles of buffer exchanges was reconstituted into the 20 mM ammonium acetate buffer to a final concentration of 80 μ M.

The synthesized iNOS peptide was desalted using peptide cleanup C18 spin tubes (Agilent, Wilmington, Delaware, USA) according to the manufacture protocol. 0.1% formic acid in 50%/50% acetonitrile/water was used as activation solvent; 0.1% formic acid in water was used as equilibration/wash solvent; and 0.1% formic acid in 75%/25% acetonitrile/water was used as elution solvent. After elution, the peptide sample was dried completely on a speedvac and reconstituted into 20 mM ammonium acetate buffer to a final concentration of 400 μ M.

For analyzing *CN*F108 CaM binding with the peptide, an equal volume of the purified *CN*F108 CaM protein (80 µM in 20mM ammonium acetate) and p-iNOS (400 µM in 20 mM ammonium acetate) samples were combined with appropriate volume of CaCl₂ (8 mM) and ammonium acetate

(4 M) stock solutions, to obtain the final solution of 40 μ M CNF108 CaM, 200 μ M p-iNOS and 200 μ M CaCl₂ in 200 mM ammonium acetate (pH = 7.0) for direct infusion ESI mass spectrometry analysis. As a control, a sample containing 40 μ M CNF108 CaM and 200 μ M CaCl₂ in 200 mM ammonium acetate (pH = 7.0) was analyzed.

To acquire the native mass spectrometric data, the sample was directly infused into the HESI-II probe of a Q-Exactive Classic Orbitrap MS instrument (Thermo Scientific, San Jose, California, US) at a 5 μ L/min flow rate using a syringe pump. It was set in positive electrospray ionization mode. The ESI source spray voltage, capillary temperature, sheath gas, auxiliary gas, S-lens RF level and mass resolution were maintained at 4.0 kV, 320 °C, 7 psi, 0 psi, 50 V, and 17,500, respectively. For data analysis, intact protein masses were deconvoluted using Unidec Version 5.0.2. 10

10. Sample preparation for infrared spectroscopy

Stocks of CNF29 CaM and CNF108 CaM were prepared at 3.7 and 4.7 mM, respectively, in 50 mM Tris-Cl, pH 7.5, 1 mM CaCl₂. Samples for infrared (IR) spectroscopic analysis of individual CNF29 CaM and CNF108 CaM were prepared by dilution of stocks to 750 μM in 50 mM Tris-Cl, pH 7.5, 1 mM CaCl₂.

Samples of CaM co-expressed with full-length iNOS were prepared in 50 mM Tris-Cl, pH 7.5, 150 mM NaCl, 1 mM DTT, 4 μ M H₄B, 10% glycerol. For IR analysis, sample concentration of full length iNOS holoprotein co-expressed with *CN*F108 CaM and *CN*F29 CaM were ~ 294 μ M and 186 μ M, respectively. Because NOS is a homodimer, the effective concentrations of the *CN* probe were ~ 588 μ M and 372 μ M for *CN*F108 CaM and *CN*F29 CaM, respectively.

Samples of CaM co-expressed with iNOS oxyFMN were prepared in 50 mM Tris-Cl, pH 7.5, 150 mM NaCl, 1 mM DTT, 4 μ M H₄B, 10% glycerol. For IR analysis, sample concentrations of iNOS oxyFMN co-expressed with *CN*F108 CaM or *CN*F29 CaM were ~ 277 μ M and 200 μ M, respectively.

The iNOS peptide (p-iNOS) (Genemed Synthesis, Inc. San Antonio, TX, USA Lot# 128072, MW 2615) was dissolved into 50 mM Tris, pH 7.5, 6 mM CaCl₂ to obtain stocks at concentration of 4.7-5.0 mM. For IR analysis, *CN*F108 CaM and p-iNOS peptide were mixed in a 1:1 concentration ratio to final concentrations of 250 μM.

To prepare samples for IR spectroscopy, $\sim 12~\mu L$ was placed between 2 mm thick CaF₂ windows (uncoated, New Wave Optics), separated by a Teflon spacer of thickness 38 μm . Temperature-dependent spectra for CNF29 and CNF108 CaM were acquired at 750 μM in 50 mM Tris-Cl, pH 7.5, 3 mM CaCl₂. Sample temperature was maintained to $\pm 0.1~^{\circ}C$ with a custom-fabricated sample cell equipped with an integrated heater and thermostat.

11. Infrared spectroscopy measurements and analyses

Infrared spectroscopy was performed with a Cary 670 FT IR spectrometer (Agilent, Santa Clara, CA, USA), equipped with a liquid N₂-cooled mercury-cadmium-telluride detector. Before

recording each interferogram, the system was purged with dry nitrogen for 20 minutes. Unlabeled CaM at corresponding concentration as the sample containing the CNF label was used to obtain the background data. A band pass filter (Spectrogon, Mountain Lakes, NJ, 4000-5000 nm) was used to limit the source bandwidth. Each interferogram was the average of 5000 scans acquired with a spectral resolution of 2 cm⁻¹. The interferograms were apodized using a 4-term Blackman-Harris function and extended with a zero-filling factor of 8. Fourier transforms were performed using the Mertz phase correction algorithm. At least triplicate spectra using distinct samples were obtained.

To remove a slowly varying baseline, a polynomial was fitted to the spectral region excluding the absorption and subtracted from the spectrum (Matlab, R2018b). Figure S11 illustrates this process using as representative triplicate data set of spectra acquired for CNF108 for which we posit two overlapping absorptions. Second derivative spectra were calculated to identify the presence of multiple component bands (Figure S12).

The absorption of the baseline-corrected spectra was fit to one or a superposition of two Gaussian

functions. $A(v) = \sum_{i=1,2} A_{io} e^{-\left(\frac{(v-v_{io})}{\sigma_i}\right)^2}$, where A_o is the amplitude of the absorption band, v_o is the center frequency, and σ is the standard deviation (full width half max = $\sqrt{2 \ln 2} \sigma$). For CNF29 CaM, the spectra of all samples were well fit by single Gaussian band (Figure 2, Table S4). Due to the simplicity of the spectrum of CNF29, we used it to assess alternate lineshape models (Figure S14). A Lorentzian lineshape, $A(\nu) = A_o \frac{1}{1 + \left(\frac{(\nu - \nu_o)}{\sigma}\right)^2}$, clearly yields a poorer fit. A Voigt lineshape was approximated by $A(\nu) = A_L \frac{1}{1 + \left(\frac{(\nu - \nu_o)}{\sigma}\right)^2} + A_G e^{-\left(\frac{(\nu - \nu_o)}{\sigma}\right)^2}$, where A_L and A_G are the amplitudes

was approximated by
$$A(\nu) = A_L \frac{1}{1 + \left(\frac{(\nu - \nu_0)}{\sigma}\right)^2} + A_G e^{-\left(\frac{(\nu - \nu_0)}{\sigma}\right)^2}$$
, where A_L and A_G are the amplitudes

of the Lorentizan and Gaussian components, respectively. The approximated Voigt fit is dominated by the Gaussian component (A_L is 3% and A_G is 97%). Therefore, a Gaussian line shape was used in all subsequent modeling.

In contrast to CNF29, all spectra for CNF108 CaM best fit to a superposition of two Gaussian functions (Figure 2). The frequencies of the two Gaussian components are approximately the same among the samples, despite that the Gaussian parameters were allowed to vary unrestrictedly. The one exception to this occurred when fitting the spectrum of the complexes with iNOS, the center frequency of the band at higher frequency, due to its small contribution, was fixed to match frequency found for unligated CNF108 CaM.

Spectra of CNF29 CaM acquired at varying temperature were similarly well fit by a single Gaussian band. The linewidth of the absorption is approximately independent of temperature, while the center frequency shifts lower with temperature increase, by approximately 2 cm⁻¹ over the 40°C temperature range (Figure S15). For CNF108 CaM, the spectra show two components at lower temperature (30-55°C), but at higher temperature are well modeled as a single band (60-70°C). The band at lower frequency found for samples at 30°C upshifts slightly to higher frequency with increasing temperature (2 cm⁻¹ over 40°C). The band at higher frequency found for samples at 30°C disappears with increasing temperature with a transition midpoint of approximately 55°C (Figure **S16**).

12. Molecular dynamics simulations

Preparation and execution of the molecular dynamics (MD) simulations utilized computational resources of Big Red 3 at Indiana University. Simulations were performed using the AMBER 20 software package, which employed the ff14SB force-field. The charges for the *CNF* were derived via the R.E.D. Server. Server. Server was introduced at V108 into the crystal structure of CaM complexed with p-nNOS (PDB ID: 2060) using Chimera UCSF. The sequence of p-nNOS was then mutated to that of p-iNOS to generate the starting model for the complex of *CNF*108 CaM with p-iNOS. Force field library files for the *CNF* and Amber topology and coordinate files for *CNF*-labeled CaM with p-iNOS were generated via the LEaP program. To solvate the protein, a 12 Å octahedron of TIP3 water was included, and Na⁺ counter ions were added to neutralize the charges of the system.

The particle mesh Ewald summation method with a non-bonded cut-off of 12 Å was employed for long-range interactions and the SHAKE procedure was used to constrain all bonds involving hydrogen atoms. A Langevin thermostat was used with a collision frequency of 2 ps⁻¹. The energy of *CNF*108 CaM-p-iNOS complex was minimized using 2500 steps of the steepest-descent algorithm and 1000 subsequent steps of conjugate gradient. The system was then heated to 300 K over 2 ns in 2 fs steps and allowed to equilibrate under the control of a Langevin thermostat. Data were acquired from six trajectories of 2 ns duration with 2 fs steps after the temperature and RMSD had converged (shown in Figure S17). The trajectories were visualized using Visual Molecular Dynamics (VMD).¹⁶ The data presented in this work were average of the six trajectories.

The MD trajectories were analyzed using the CPPTRAJ¹⁷ program of Amber20. The rmsd from the starting structures increases over the first 400 ps then fluctuates around 2 Å over the course of the trajectories; the *CNF* thus does not appear to induce substantial change to the structures of the complex. We then analyzed the trajectories to assess two commonly attributed origins of solvatochromism for the cyano stretch vibration hydrogen bonding and a Stark effect due to the local electric field. ^{18,19} Analysis of hydrogen bonding involving the cyano nitrogen of *CNF*108 to solvent or protein moieties during the MD simulations was conducted using a distance cutoff of 3 Å (Table **S5**). This analysis indicates negligible hydrogen bonding (1.6% of frames). The electric field projected along the cyano bond was determined as previously described (Figure **S18**). ¹³

Alternately, we considered short-range packing interaction as a source of solvatochromism. Our prior analysis of *CNF* in cytochrome P450cam found the vibrational frequency to be most correlative with proximity of neighboring atoms.²⁰ To analyze the environments of *CNF*108 in the complexes of CaM with p-iNOS, the atoms approaching the cyano nitrogen within 5 Å was determined (Table **S6**). Frequent short-range approach of *CNF*108 and residues Val35, Ser38, and Leu39 of the N-lobe, Val 91 and Leu 112 of the C-lobe, and Val 159 of the peptides is observed.

Because the same two absorption bands (approximately same frequency) are observed for *CNF*108 CaM in the absence of ligand and when associated with iNOS, they likely report on a feature of the environment within the C-lobe, which is common among all states. Note that in absence of ligand, the majority population of CaM is thought to adopt an extended structure in which the N-lobe and C-lobe are dissociated.²¹ Histograms of the distance of the cyano nitrogen of *CNF*108 to residues

V91, L112, F141 and M144 of the C-lobe illustrate the distinct environments of the CN in the complex with p-iNOS (Figure **S19a**).

The average structures of CaM in the complexes with p-iNOS from our MD or prior structural studies differ by interhelical displacements. Similar conformational changes within and between the EF hands of the N- and C-terminal lobes are well known to occur during the transition from the apoprotein to holoprotein upon binding of Ca²⁺. Several order parameters have been proposed to describe the conformational changes. We analyzed the average structures from the MD simulations via the online analysis tools provided by Hiroshi Kawasaki et al. at http://calcium.sci.yokohama-cu.ac.jp/efhand.html,²² in which the angle between helices within an EF hand is described by parameter dE(phi), and the angle between the EF hands in the N- or C-lobe is described by parameter, dF(phi) (Table S7).



13. Figures and Tables

- Figure S1. Absorption spectra of wild type, CNF108, and CNF29 CaM proteins.
- **Figure S2.** Tandem mass spectrum of trypsin-digested *CN*F108 CaM confirming the site-specific incorporation of *CN*F at position 108.
- **Figure S3.** Tandem mass spectrum of trypsin-digested *CN*F29 CaM confirming the site-specific incorporation of *CN*F at position 29.
- **Figure S4.** Tandem mass spectrum of trypsin digested CaM co-expressed with full-length iNOS protein confirming the site-specific incorporation of *CNF* at position 108.
- **Figure S5.** Tandem mass spectrum of trypsin digested CaM co-expressed with full-length iNOS protein confirming the site-specific incorporation of *CNF* at position 29.
- Figure S6. Deconvoluted mass spectra of intact CNF108 CaM protein.
- **Figure S7.** Intact protein mass spectrum of denatured *CNF*108 CaM protein co-expressed with full-length iNOS protein.
- **Figure S8.** Intact protein mass spectrum of denatured *CN*F29 CaM.
- **Figure S9.** Intact protein mass spectrum of denatured *CN*F29 CaM co-expressed with full-length iNOS protein.
- **Figure S10.** Native protein mass spectroscopic analysis of ligand binding by CNF108 CaM.
- **Figure S11.** Illustration of baseline correction of the unprocessed absorption spectra using three sets of data for *CN*F108 CaM.
- **Figure S12.** Absorption spectra and corresponding second derivative spectra for *CN*F108 CaM in the absence and presence of full length iNOS isoenzymes.
- **Figure S13.** FT IR spectra of *CN*F108 CaM when associated with p-iNOS.
- **Figure S14.** Comparison of fits of absorption band for *CN*F29 CaM to Gaussian, Lorentzian, and approximated Voigt lineshapes.
- **Figure S15.** IR spectra of individual *CN*F29 CaM at varying temperature.
- **Figure S16.** IR spectra of individual *CN*F108 CaM at varying temperature.
- **Figure S17.** Root-mean-square-deviation from starting structure over the six trajectories of *CNF*108 CaM in complexation with p-iNOS.
- **Figure S18.** Histograms of the projection of electric field along the cyano bond determined from MD simulations of *CN*F108 CaM in complex with p-iNOS.
- **Figure S19.** Histograms of distance between cyano nitrogen of *CN*F108 and select residues of CaM during MD simulations of the complex with p-iNOS and the average structures of the C-lobe from a representative trajectory of *CN*F108 CaM in complexation with p-iNOS.
- **Table S1.** Extinction co-efficient of wt, CNF108, and CNF29 CaM proteins.
- **Table S2.** NO production rate of iNOS enzyme in the presence of *CNF*-labelled CaM proteins.
- **Table S3.** Sequences of peptides containing CaM recognition elements of iNOS isoform.
- **Table S4.** Parameters from Gaussian fit to spectra of *CNF*-labeled CaM.
- **Table S5.** Hydrogen bonding interactions of residue *CN*F108 during MD simulations
- **Table S6.** Residues that approach *CNF* within 5 Å during MD simulations.
- **Table S7.** Average EF-hand parameters of the C-lobes of CaM in the complex with p-iNOS.

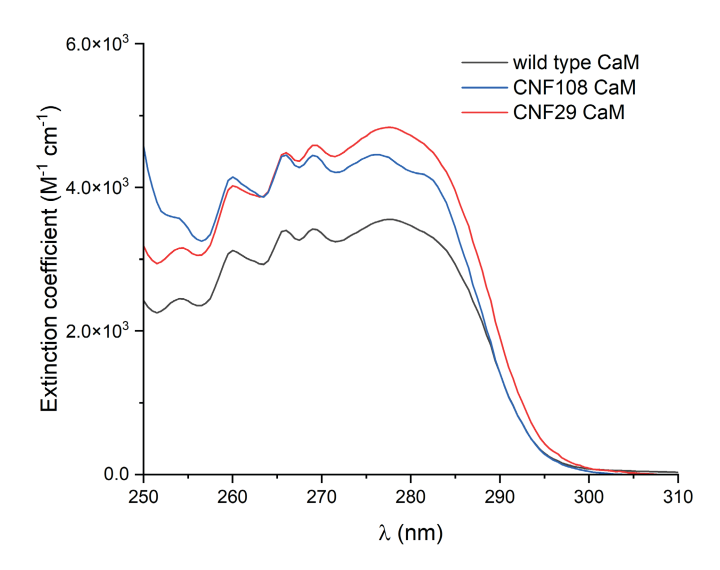


Figure S1. Absorption spectra of wild type, *CNF* 108 and *CNF* 29 CaM proteins. The extinction coefficients of *CNF* CaM proteins are in general larger than the wild type. Also of note is that *CNF* 108 CaM exhibits a clearer shoulder peak at 280 nm, in comparison to the wild type. These differences arise from the absorption of the incorporated *CNF* residue in the UV region.²³

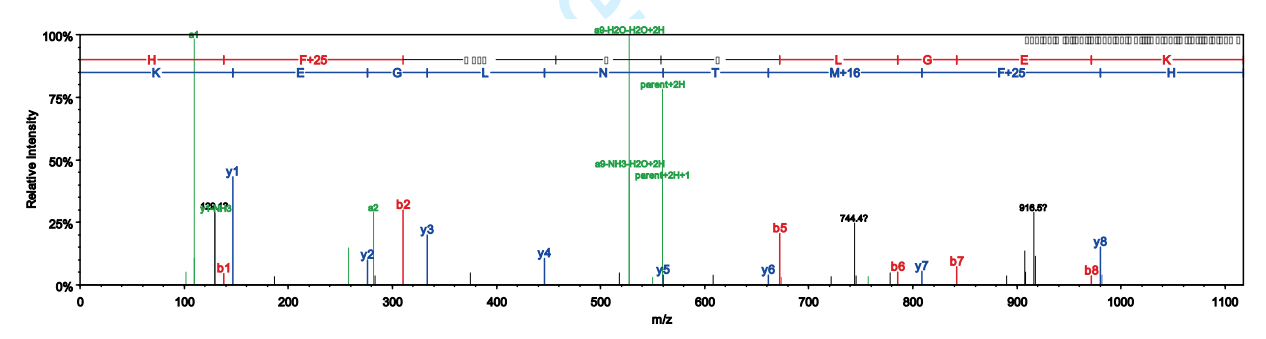


Figure S2. Tandem mass spectrum of trypsin-digested *CN*F108 CaM confirming the site-specific incorporation of *CN*F at position 108. The *CN*F108 addition is definite since both the N-terminal and C-terminal product ions contain cyano mass (+25).

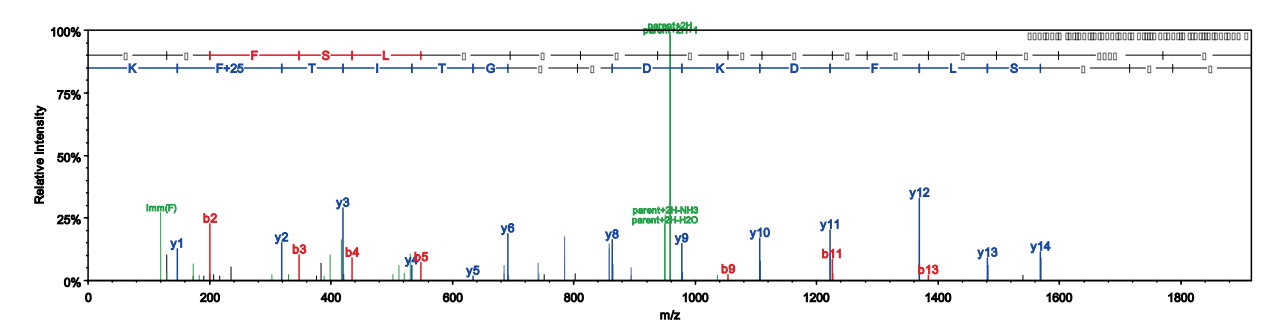


Figure S3. Tandem mass spectrum of trypsin-digested *CN*F29 CaM confirming the site-specific incorporation of *CN*F at position 29.

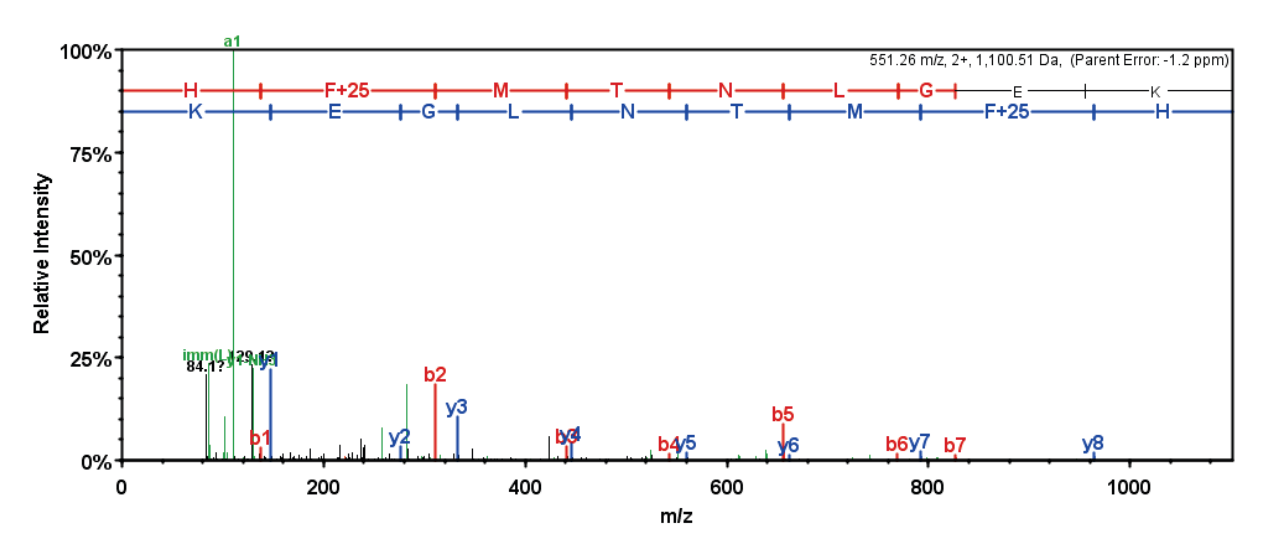


Figure S4. Tandem mass spectrum of trypsin-digested *CNF*108 CaM co-expressed with full-length iNOS protein confirming the site-specific incorporation of *CNF* at position 108.

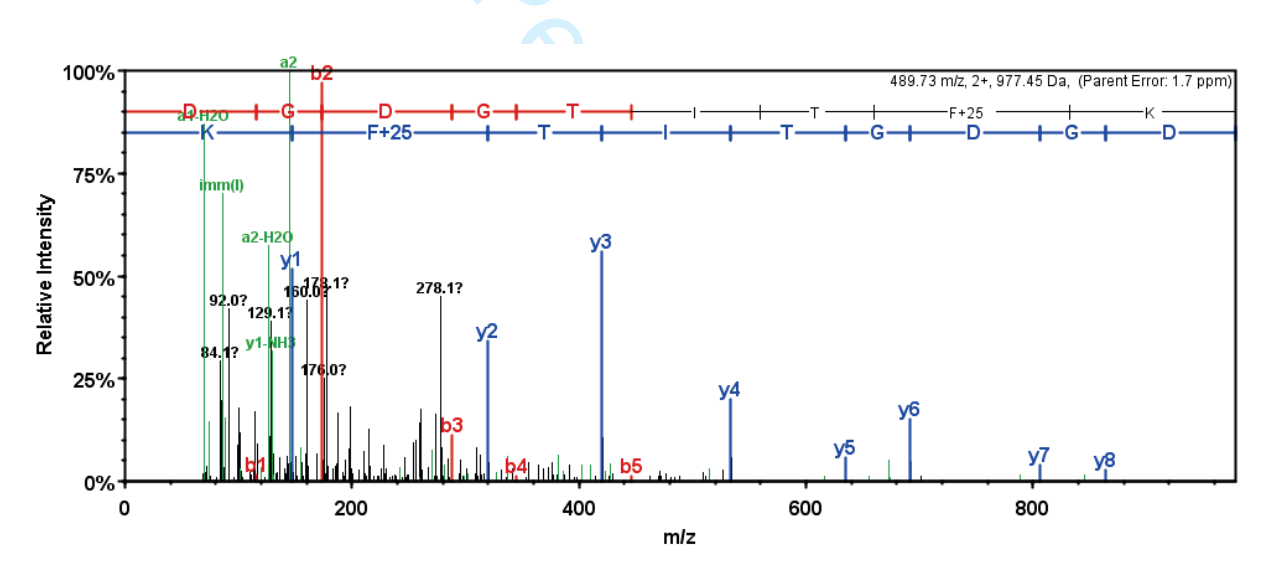


Figure S5. Tandem mass spectrum of trypsin-digested *CN*F29 CaM co-expressed with full-length iNOS protein confirming the site-specific incorporation of *CN*F at position 29.

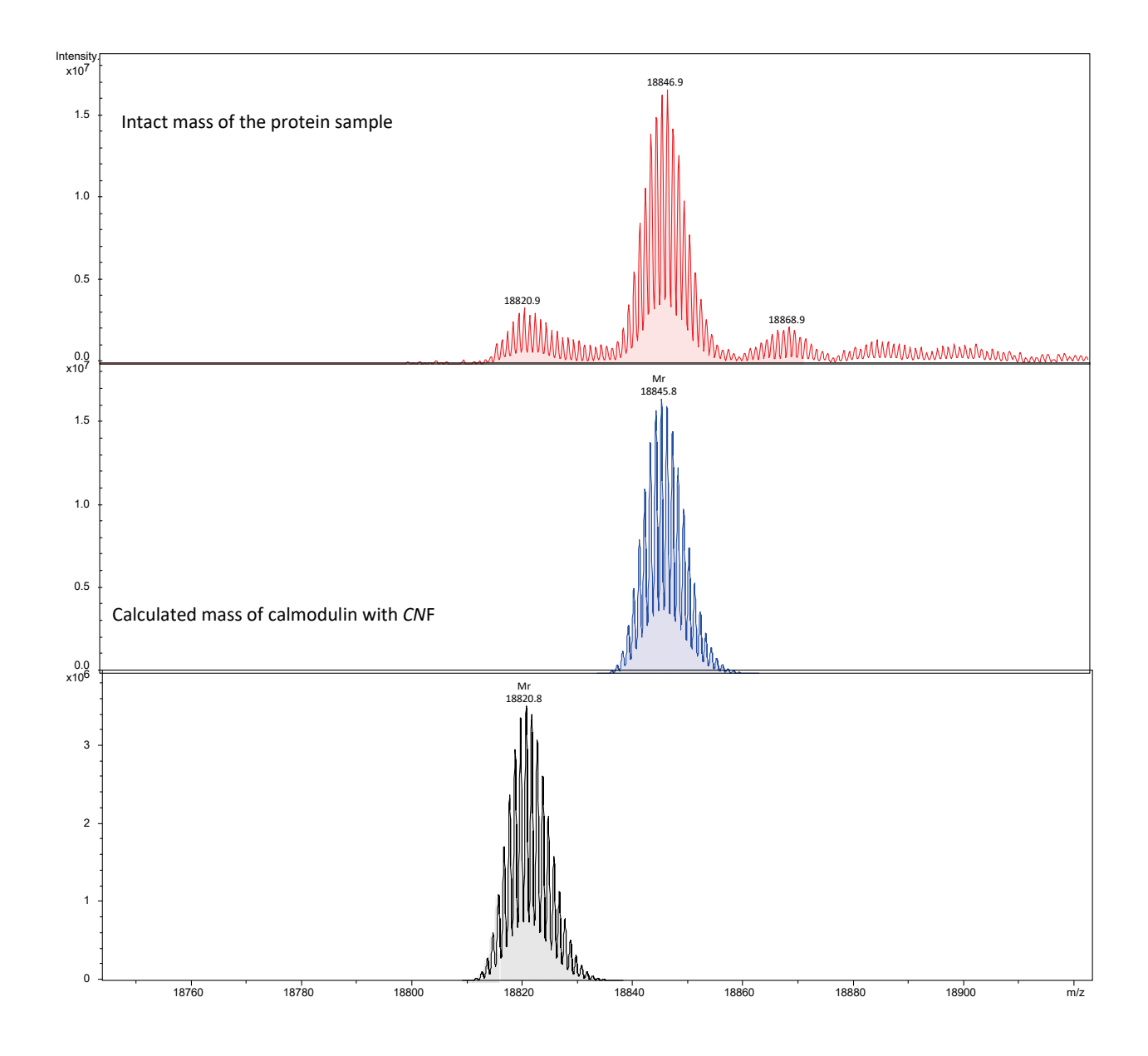


Figure S6. Deconvoluted mass spectra of intact CNF108 CaM. The intact mass of protein was determined by UPLC-MS. Desalting and LC separation was carried out using a Bruker's Elute UPLC on a 100×2.1 mm ACQUITY BEH 1.7 μ m C4 column and a 38-min analytical gradient. Eluted proteins were directly introduced to a Bruker solariX MRMS mass spectrometer (FT-ICR) via an ESI source. All the instrument control and sample tables were controlled by using Compass HyStar 4.1 software. The raw data was processed and deconvoluted by the Maximum Entropy algorithm in Compass Data Analysis software. This protein contains a C-terminal His6 tag, and its mass is thus different from the CNF108 CaM protein co-expressed with iNOS (see Figure S7 below).

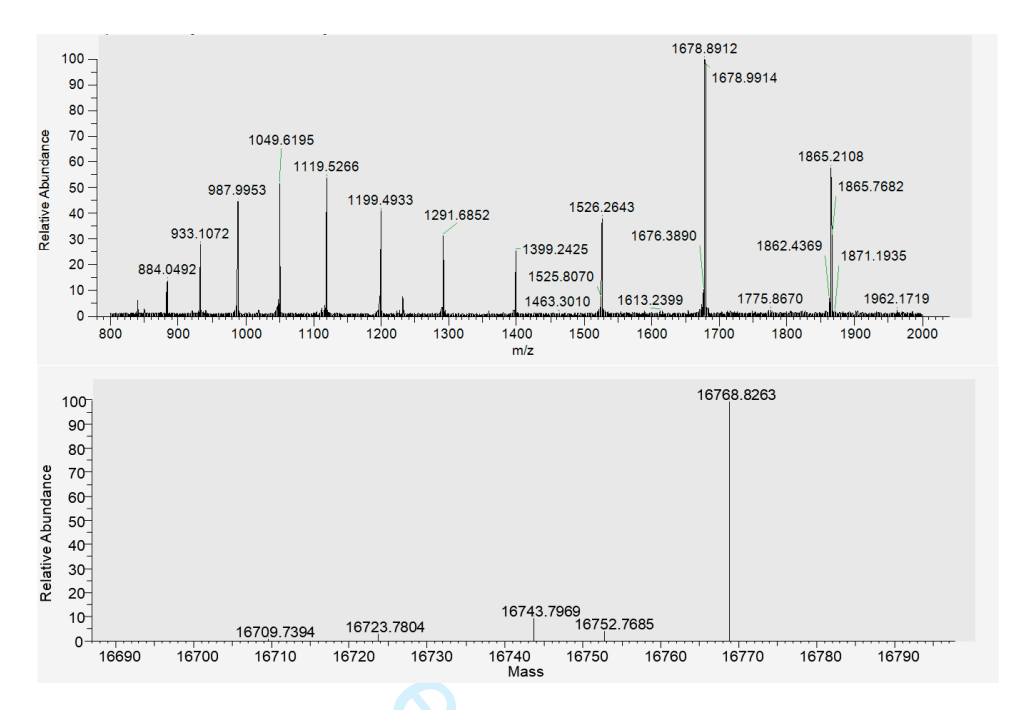


Figure S7. Intact protein mass spectrum of denatured *CN*F108 CaM co-expressed with full-length iNOS protein. The CaM protein was dissociated from the CaM-iNOS complex prior to the direct infusion. Top: averaged raw mass spectrometric data for the interested peak in the chromogram; bottom: deconvoluted mass spectrum for the intact *CN*F108 CaM. Note that the *CN*F108 CaM here does not contain a His₆ tag.

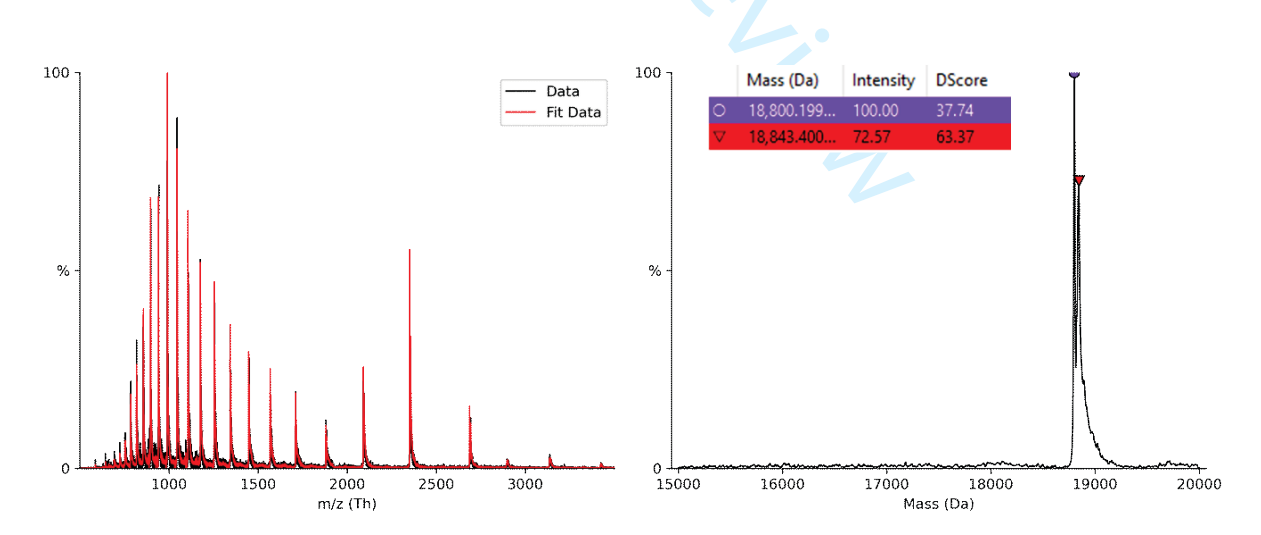


Figure S8. Intact protein mass spectrum of denatured *CN*F29 CaM. The data were collected on a Waters Xevo G2-S QTof instrument. The raw data were deconvoluted using UniDec to generate the spectra in the right panel. This protein contains a C-terminal His₆ tag, and its mass is thus different from the *CN*F29 CaM protein co-expressed with iNOS (see Figure S9 below).

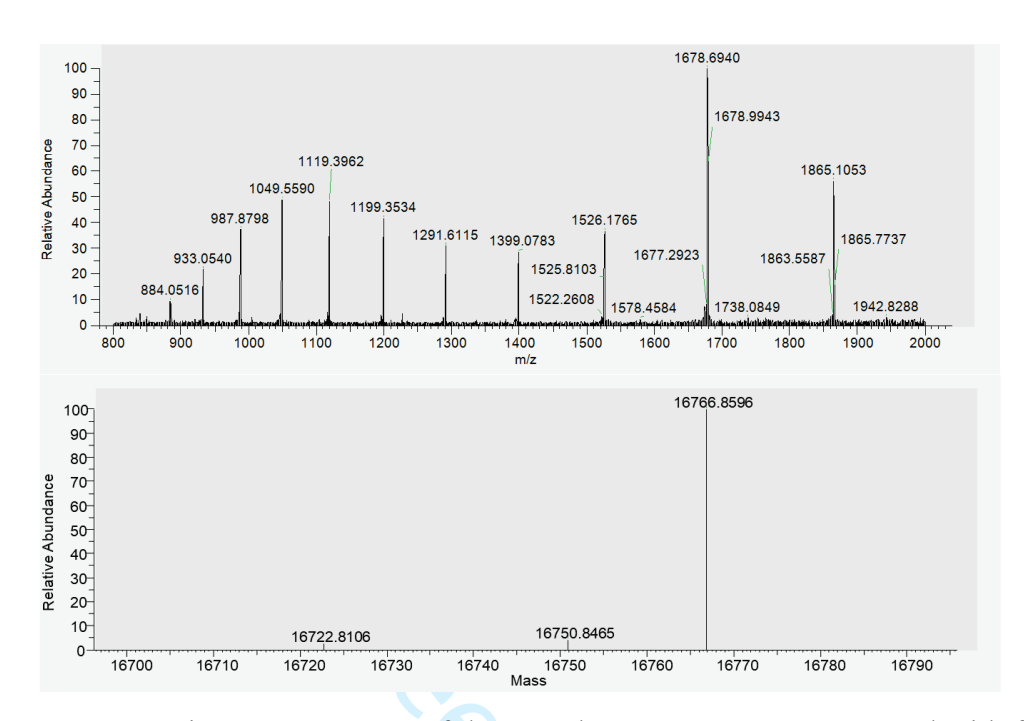


Figure S9. Intact protein mass spectrum of denatured *CN*F29 CaM co-expressed with full-length iNOS protein. The CaM protein was dissociated from the CaM-iNOS complex prior to the direct infusion. Top: averaged raw mass spectrometric data for the interested peak in the chromogram; bottom: deconvoluted mass spectrum for the intact *CN*F29 CaM protein. Note that the *CN*F29 CaM here does not contain a His₆ tag.

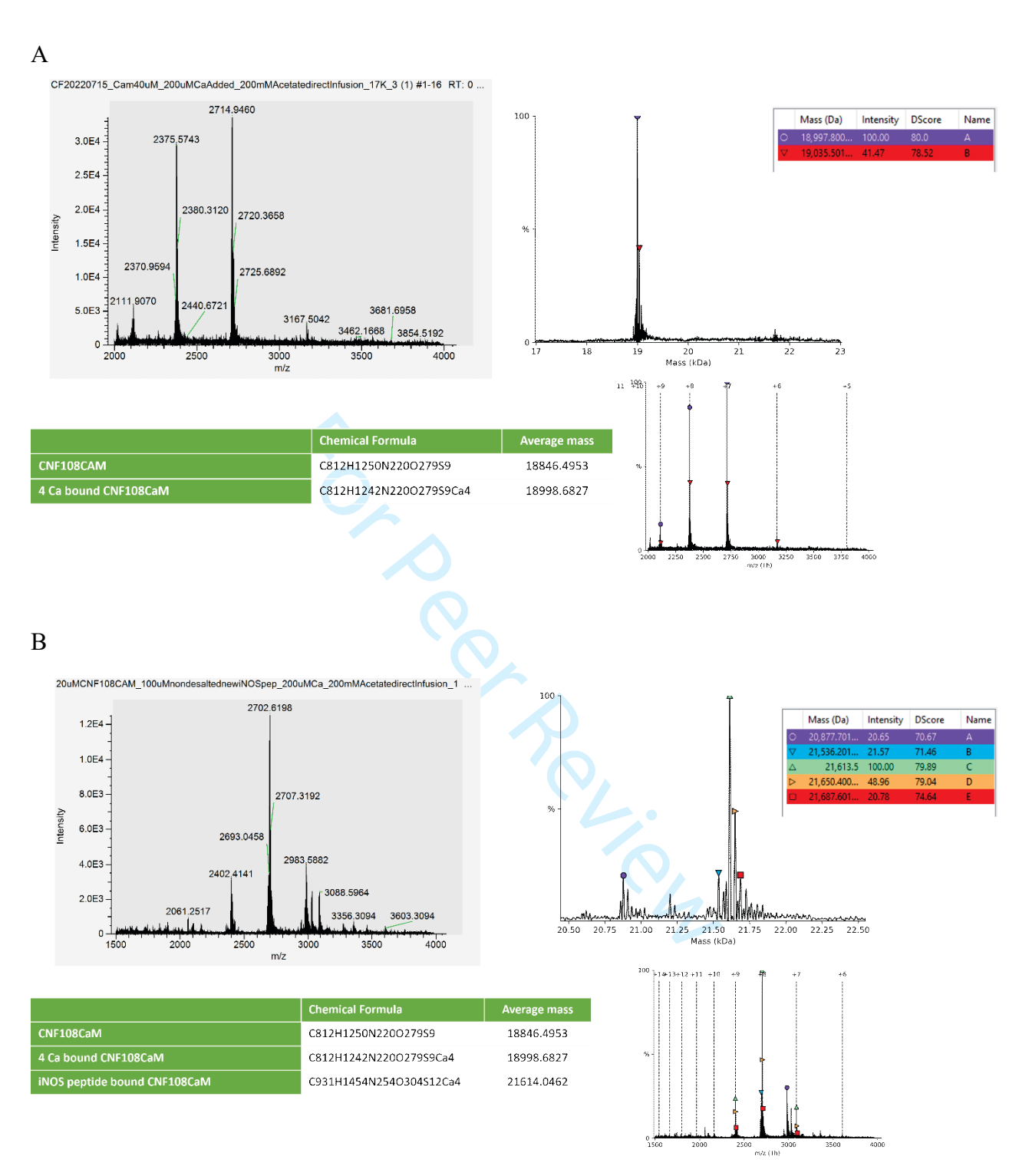


Figure S10. Native protein mass spectroscopic analysis of ligand binding by *CN*F108 CaM. Native mass spectra for (A) Ca²⁺-*CN*F108 CaM, and (B) Ca²⁺-*CN*F108 CaM with added iNOS-peptide (RREIPLKVLVKAVLFACMLMRK). The iNOS peptide can bind to 2Ca²⁺-*CN*F108 CaM, while the 4Ca²⁺-CaM form dominates.

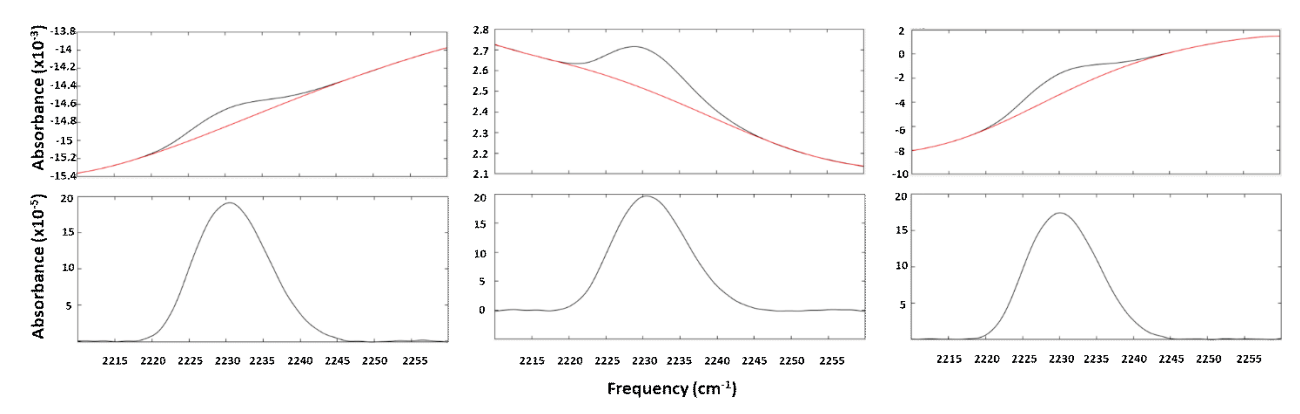


Figure S11. Illustration of baseline correction of the unprocessed absorption spectra using three sets of data for *CN*F108 CaM. A polynomial of order 4-6 is fit to the spectral regions excluding the absorption band (top panels). The polynomial is subtracted from the unprocessed absorption spectra, resulting in baseline-corrected spectra (bottom panels).

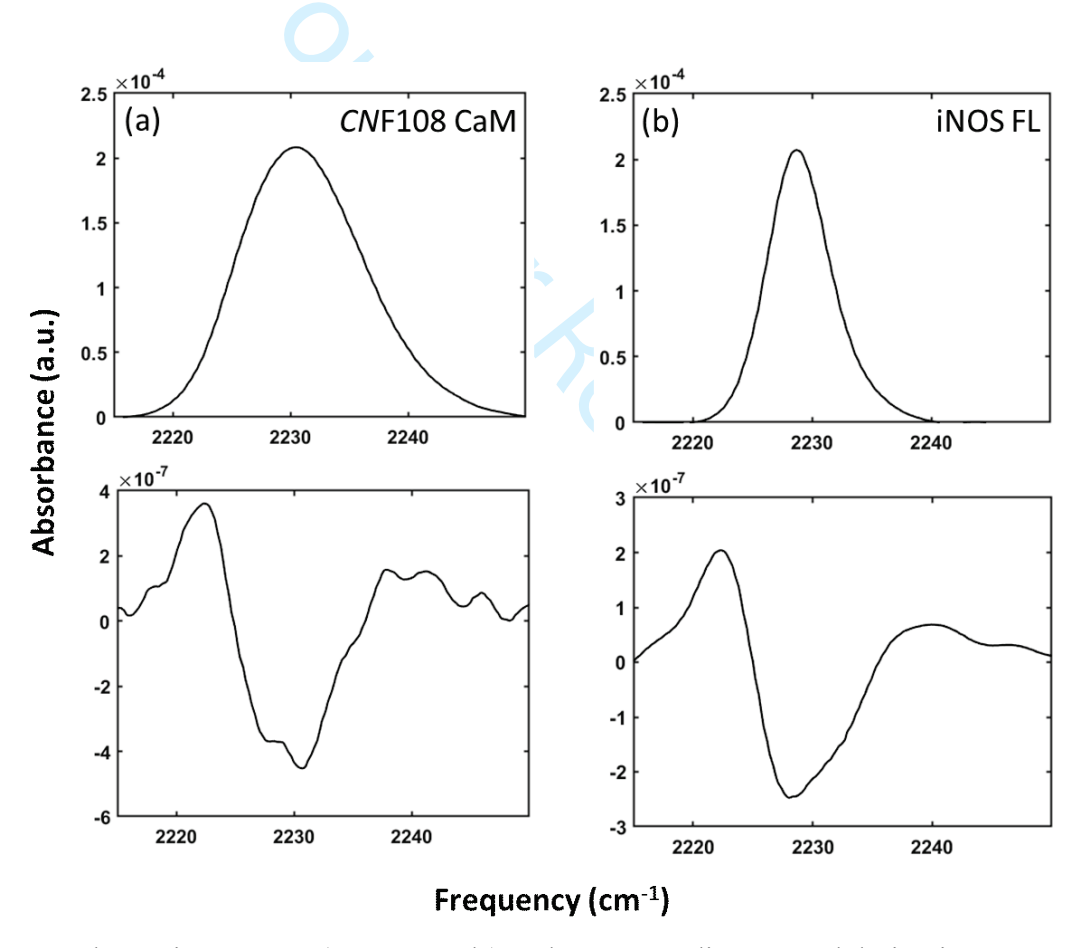


Figure S12. Absorption spectra (upper panels) and corresponding second derivative spectra (lower panels) for *CNF*108 CaM in the (a) absence, and (b) presence of full length (FL) iNOS isoenzyme. The appearance of two minima in the second derivative spectra is indicative of the presence of two bands in the absorption spectra.

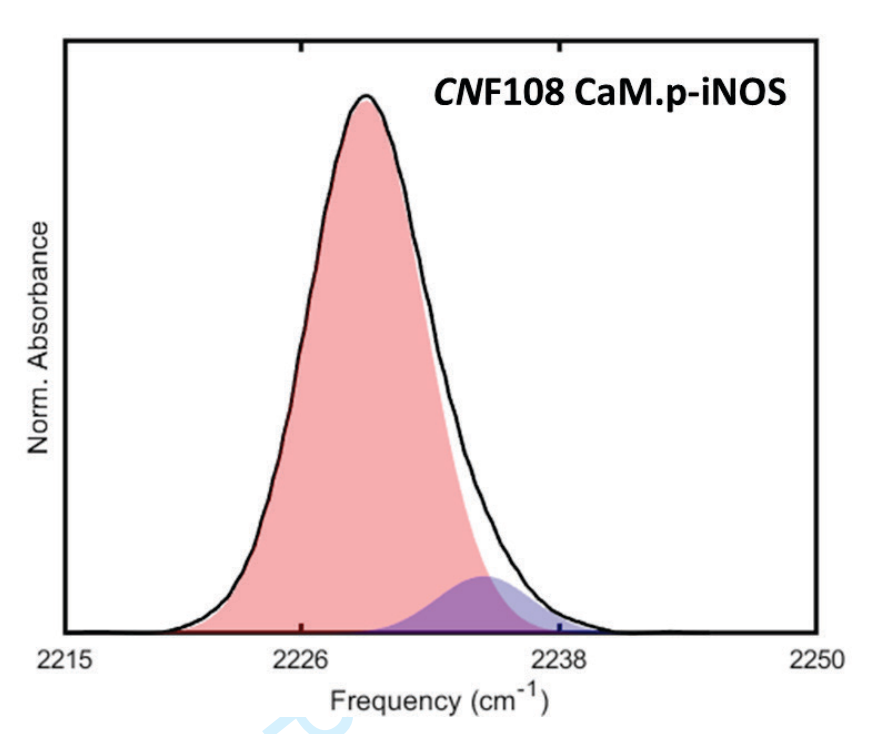


Figure S13. IR spectra of *CN*F108 CaM when associated with p-iNOS.

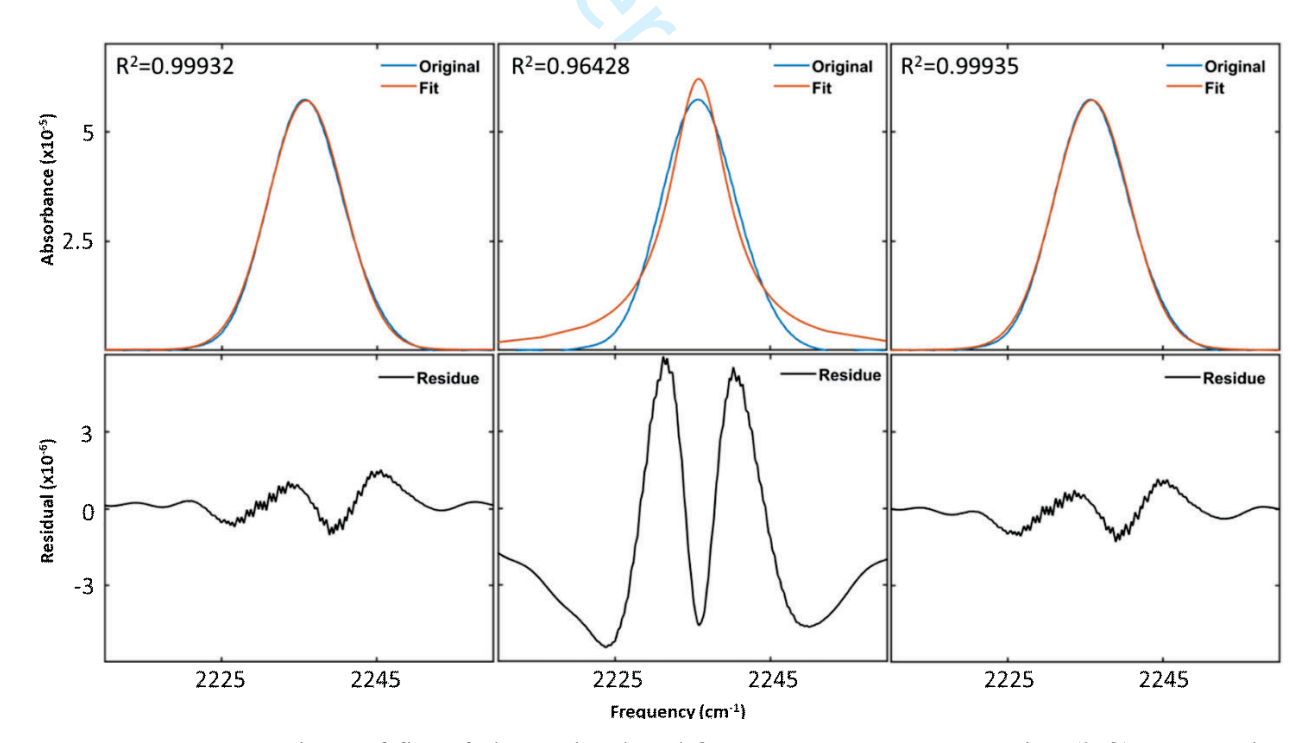


Figure S14. Comparison of fits of absorption band for *CN*F29 CaM to Gaussian (left), Lorentzian (middle), and approximated Voigt (right) lineshape.

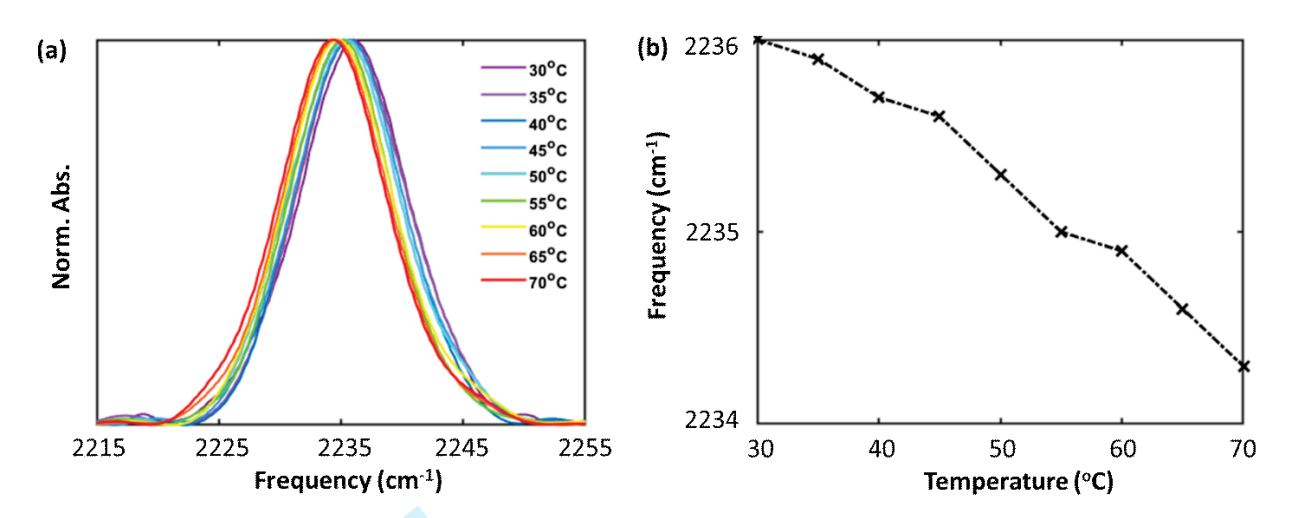


Figure S15. Temperature-dependent IR analysis of individual *CN*F29 CaM. (a) IR spectra of *CN*F29 CaM at varying temperature. (b) Plot of shift in center frequency with increasing temperature.

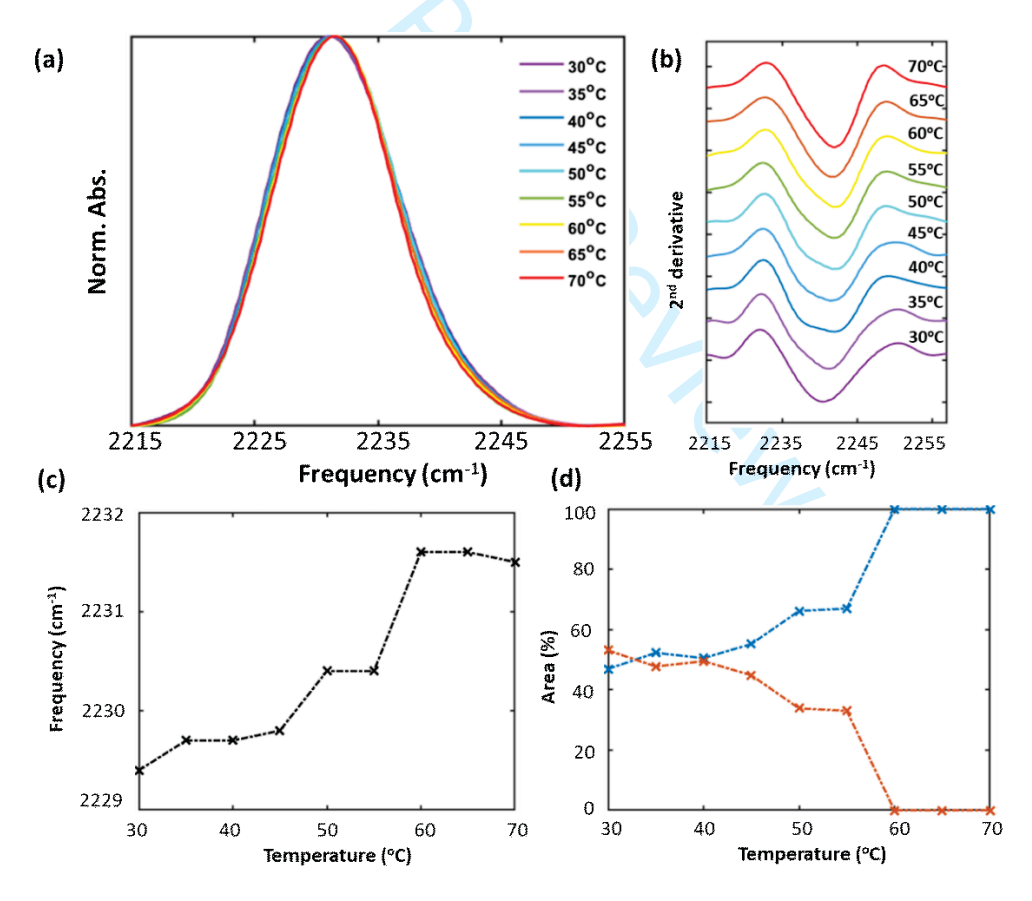


Figure S16. Temperature-dependent IR analysis of individual *CN*F108 CaM. (a) IR absorption spectra and (b) second derivative spectra at varying temperature. (c) Plot of shift in center frequency of lower frequency band with increasing temperature. (d) Plot of relative areas of lower (blue) and higher (orange) frequency bands with temperature.

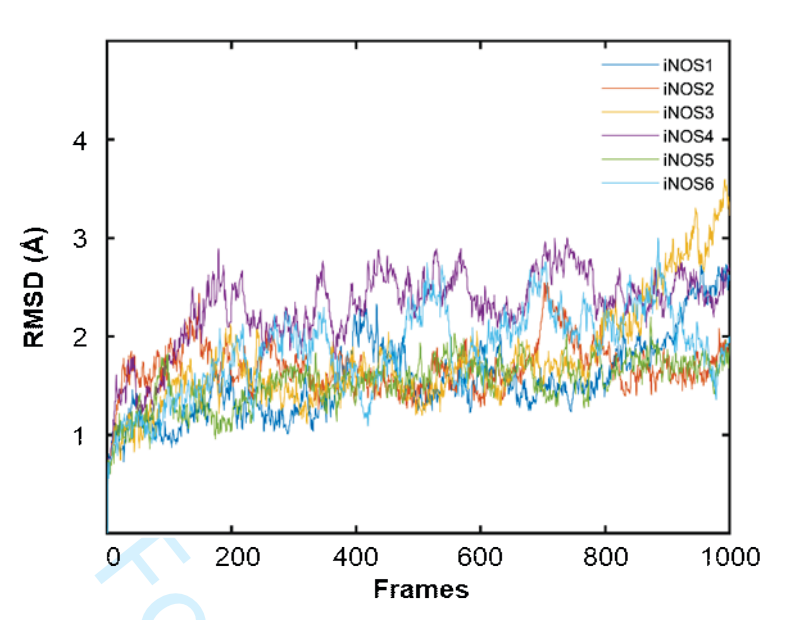


Figure S17. Root-mean-square-deviation from starting structure over the six trajectories of *CNF*108 CaM in complexation with p-iNOS.

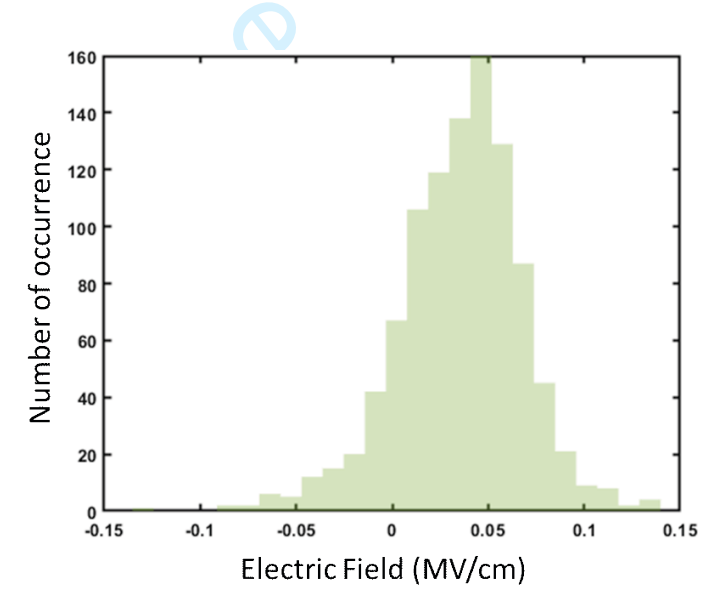


Figure S18. Histogram of the projection of electric field along the cyano bond determined from MD simulations of *CN*F108 CaM in complexation with p-iNOS.

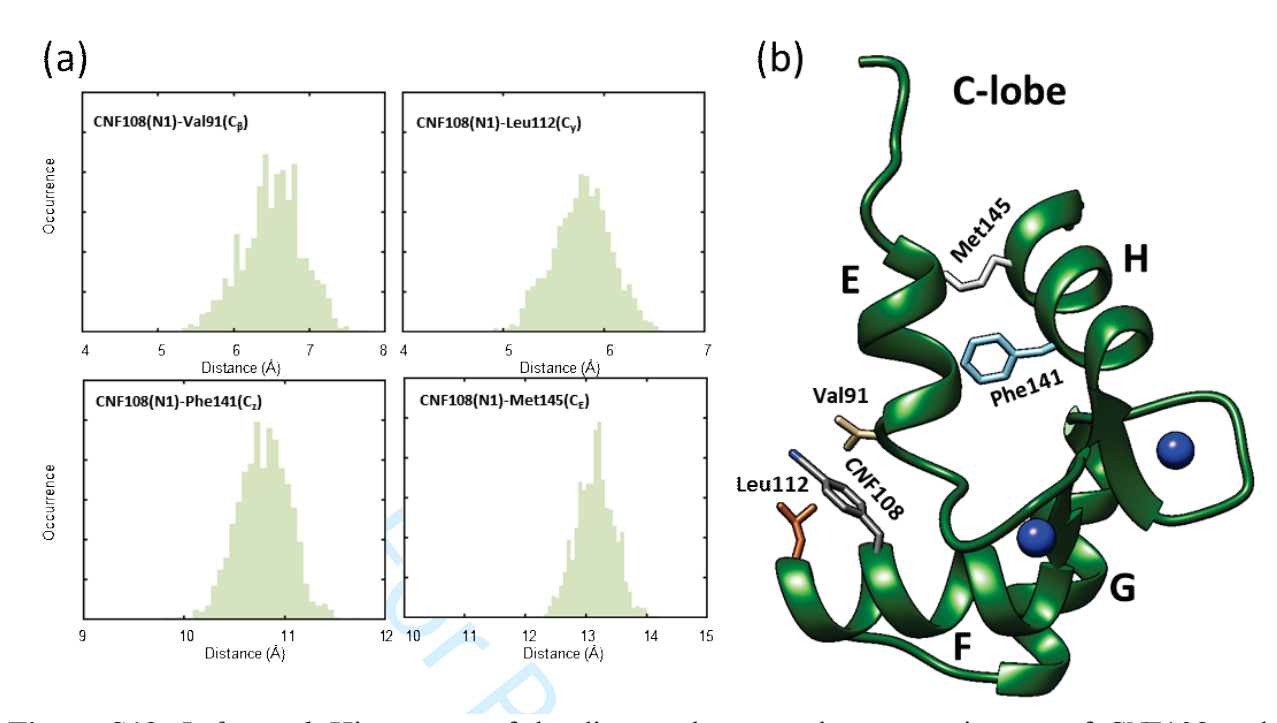


Figure S19. Left panel: Histograms of the distance between the cyano nitrogen of CNF108 and select residues of CaM for the complexes with p-iNOS. The top panels show distance to adjacent residues of the C-lobe. The bottom panels show distance to residues of helix H to illustrate the wider groove formed in the complex with p-iNOS. Right panel: The ribbon models of the average structures of the C-lobe from a representative trajectory of CNF108 CaM in complex with p-iNOS. Side chains are shown as sticks for residue CNF108 and additional residues that illustrate the distinct environments of the CN probe. Ca²⁺ ions are shown as blue spheres.

7.04

Table S1. Extinction co-efficient of CaM proteins at 277 nm.^a

| CaM protein | ε (M ⁻¹ cm ⁻¹) |
|---------------|---------------------------------------|
| wild type CaM | 3459.0 ± 49.6 |
| CNF108 CaM | 4436.9 ± 96.3 |
| CNF29 CaM | 4830.5 ± 79.2 |

^a The protein concentration was measured using Pierce 660nm Protein Assay Kit in triplicate. The extinction coefficient was then calculated from the UV-vis spectra and the concentration.

Table S2. Rate of NO synthesis by the iNOS holoenzyme co-expressed with *CNF*-labelled CaM.

| CaM | NO synthesis (min ⁻¹) |
|----------------|-----------------------------------|
| wild type | 62 ± 4 |
| <i>CN</i> F108 | 57 ± 2 |
| CNF29 | 55 ± 3 |

Table S3. Sequences of peptides containing CaM recognition element of iNOS isoform.^a

| Peptide | Sequence |
|---------|------------------------|
| iNOS | RREIPLKVLVKAVLFACMLMRK |

^a The peptide was synthesized by Genemed Synthesis, Inc.; purity > 95%.

Table S4. Parameters from Gaussian fit to spectra of *CNF*-labeled CaM.

| Sample | v_0 (cm ⁻¹) | FWHM ^a (cm ⁻¹) | Area (%) |
|------------------------|--------------------------------------|---------------------------------------|----------------------------------|
| | CNF29 CaM | | |
| CNF29 CaM | $2235.8 \pm \! 0.02$ | 11.3 ± 0.4 | 100 |
| CNF29 CaM·iNOS FL | 2235.9 ± 0.1 | 11.4±0.11 | 100 |
| CNF29 CaM·iNOS oxyFMN | 2236.2±0.04 | 11.2±0.21 | 100 |
| <i>CNF</i> 108 CaM | | | |
| CNF108 CaM | 2229.4 ± 0.1 2234.3 ± 0.1 | 9.8 ± 0.1 12.4 ± 0.1 | 48.0 ± 0.9 52.0 ± 0.9 |
| CNF108 CaM·iNOS FL | 2228.7 ±0.03 | 5.8 ± 0.1 | 89.6 ±0.3 |
| | 2233.9 ± 0.3 | 5.7 ± 0.1 | 10.4 ± 0.3 |
| CNF108 CaM·iNOS oxyFMN | 2228.7±0.02 | 5.7±0.03 | 92.0±0.3 |
| | 2233.7±0.11 | 5.2 ± 0.14 | 8.0 ± 0.3 |
| CNF108 CaM·p-iNOS | 2229.0 ± 0.1 2234.4 ± 0.3 | 6.4 ± 0.2 5.0 ± 0.6 | 91.4 ±3.2 8.6 ±3.2 |

^a full-width-half-maximum

Table S5. Hydrogen bonding interactions of residue *CN*F108 with the water solvent and other residues observed across 6000 MD frames.

| CaM-NOS Complex | Water | Residues |
|--------------------------|-------|----------|
| CaM bound p-iNOS complex | 97 | |

Table S6. Residues that approach *CNF* within 5 Å during MD simulations.

| CaM bound p-iNOS complex | | |
|--------------------------|--------|---------|
| N-Lobe | C-Lobe | Peptide |
| Leu18 | Val91 | Leu155 |
| Val35 | Leu112 | Val159 |
| Ser38 | | Ala162 |
| Leu39 | | |
| Gly40 | | |
| Gln41 | | |

Table S7. Average EF-hand parameters of the C-lobes of CaM in the complex with p-iNOS.

| Parameters | iNOS |
|-----------------------|-------------|
| Odd dE(phi) | 12.4 (1.7) |
| Average of dE(phi) | 7.0 (1.4) |
| delta dF(phi) between | 32.9 (2.1) |
| Odd and Even | |
| Odd domain | 96.5 (3.0) |
| Even domain | 111.8 (2.4) |

Note: Odd E-helix 84–91; Odd F-helix 104–111; Even E-helix 120–127; Even F-helix 140–147, The value in parentheses represent the standard deviation along 6000 trajectories.

References

- 1. Creon, A.; Josts, I.; Niebling, S.; Huse, N.; Tidow, H., Conformation-specific detection of calmodulin binding using the unnatural amino acid p-azido-phenylalanine (AzF) as an IR-sensor. *Struct Dyn* **2018**, *5* (6), 064701-12.
- 2. Feng, C.; Dupont, A. L.; Nahm, N. J.; Spratt, D. E.; Hazzard, J. T.; Weinberg, J. B.; Guillemette, J. G.; Tollin, G.; Ghosh, D. K., Intraprotein electron transfer in inducible nitric oxide synthase holoenzyme. *J Biol Inorg Chem* **2009**, *14* (1), 133-42.
- 3. Hussain, H.; Chong, N. F., Combined Overlap Extension PCR Method for Improved Site Directed Mutagenesis. *Biomed Res Int* **2016**, 2016, 8041532.
- 4. Spratt, D. E.; Newman, E.; Mosher, J.; Ghosh, D. K.; Salerno, J. C.; Guillemette, J. G., Binding and activation of nitric oxide synthase isozymes by calmodulin EF hand pairs. *FEBS J* **2006**, *273* (8), 1759-71.
- 5. Pirman, N. L.; Barber, K. W.; Aerni, H. R.; Ma, N. J.; Haimovich, A. D.; Rogulina, S.; Isaacs, F. J.; Rinehart, J., A flexible codon in genomically recoded Escherichia coli permits programmable protein phosphorylation. *Nat Commun* **2015**, *6*, 8130.
- 6. Panda, S. P.; Li, W.; Venkatakrishnan, P.; Chen, L.; Astashkin, A. V.; Masters, B. S.; Feng, C.; Roman, L. J., Differential calmodulin-modulatory and electron transfer properties of neuronal nitric oxide synthase mu compared to the alpha variant. *FEBS Lett* **2013**, *587* (24), 3973-3978.
- 7. Nancy L. Andon, S. H., Antonius Koller, Andrew J. Greenland, John R. Yates III, Paul A. Haynes, Proteomic characterization of wheat amyloplasts using identification of proteins by tandem mass spectrometry. *Proteomics* **2002**, *2* (9), 1156-1168.
- 8. Wei-Jun Qian, T. L., Matthew E. Monroe, Eric F. Strittmatter, Jon M. Jacobs, Lars J. Kangas, Konstantinos Petritis, David G. Camp II, and Richard D. Smith, Probability-Based Evaluation of Peptide and Protein Identifications.pdf. *Journal of Proteome Research* **2005**, 4, 53-
- 9. Keller, A.; Nesvizhskii, A. I.; Kolker, E.; Aebersold, R., Empirical Statistical Model To Estimate the.pdf. *Anal. Chem.* **2002**, *74*, 5383-5392.
- 10. Marty, M. T.; Baldwin, A. J.; Marklund, E. G.; Hochberg, G. K.; Benesch, J. L.; Robinson, C. V., Bayesian deconvolution of mass and ion mobility spectra: from binary interactions to polydisperse ensembles. *Anal Chem* **2015**, *87* (8), 4370-6.
- 11. Case, D. A. B., J. T.; Betz, R. M.; Cerutti, D. S.; Cheatham, T. E., III; Darden, T. A.; Duke, R. E.; Giese, T. J.; Gohlke, H.; Goetz, A. W.; Homeyer, N.; Izadi, S.; Janowski, P.; Kaus, J.; Kovalenko, A.; Lee, T. S.; LeGrand, S.; Li, P.; Luchko, T.; Luo, R.; Madej, B.; Merz, K. M.; Monard, G.; Needham, P.; Nguyen, H.; Nguyen, H. T.; Omelyan, I.; Onufriev, A.; Roe, D. R.; Roitberg, A.; Salomon-Ferrer, R.; Simmerling, C. L.; Smith, W.; Swails, J.; Walker, R. C.; Wang, J.; Wolf, R. M.; Wu, X.; York D. M.; Kollman, P. A., AMBER 2015. **2015**, *University of California, San Francisco*.
- 12. Hornak, V.; Abel, R.; Okur, A.; Strockbine, B.; Roitberg, A.; Simmerling, C., Comparison of multiple Amber force fields and development of improved protein backbone parameters. *Proteins* **2006**, *65* (3), 712-25.
- 13. Ramos, S.; Horness, R. E.; Collins, J. A.; Haak, D.; Thielges, M. C., Site-specific 2D IR spectroscopy: a general approach for the characterization of protein dynamics with high spatial and temporal resolution. *Phys Chem Chem Phys* **2019**, *21* (2), 780-788.
- 14. Vanquelef, E.; Simon, S.; Marquant, G.; Garcia, E.; Klimerak, G.; Delepine, J. C.; Cieplak, P.; Dupradeau, F. Y., R.E.D. Server: a web service for deriving RESP and ESP

- charges and building force field libraries for new molecules and molecular fragments. *Nucleic Acids Res* **2011**, *39* (Web Server issue), W511-7.
- 15. Pettersen, E. F.; Goddard, T. D.; Huang, C. C.; Couch, G. S.; Greenblatt, D. M.; Meng, E. C.; Ferrin, T. E., UCSF Chimera-a visualization system for exploratory research and analysis. *J Comput Chem* **2004**, *25* (13), 1605-12.
- 16. Humphrey, W.; Dalke, A.; Schulten, K., VMD Visual Molecular Dynamics.pdf. *Journal of Molecular Graphics* **1996**, *14*, 33-38.
- 17. Roe, D. R.; Cheatham, T. E., 3rd, PTRAJ and CPPTRAJ: Software for Processing and Analysis of Molecular Dynamics Trajectory Data. *J Chem Theory Comput* **2013**, *9* (7), 3084-95.
- 18. Adhikary, R.; Zimmermann, J.; Dawson, P. E.; Romesberg, F. E., Temperature Dependence of CN and SCN IR Absorptions Facilitates Their Interpretation and Use as Probes of Proteins. *Anal Chem* **2015**, *87* (22), 11561-7.
- 19. Boxer, I. T. S. a. S. G., Vibrational Stark Effects Calibrate the Sensitivity of Vibrational Probes for Electric Fields in Proteins. *Biochemistry* **2003**, *42*, 12050-12055.
- 20. Basom, E. J.; Maj, M.; Cho, M.; Thielges, M. C., Site-Specific Characterization of Cytochrome P450cam Conformations by Infrared Spectroscopy. *Anal Chem* **2016**, *88* (12), 6598-6606.
- 21. Johnson, C. K., Calmodulin, Conformational States, and Calcium Signaling. A Single-Molecule.pdf. *Biochemistry* **2006**, *45* (48).
- 22. Kawasaki, H.; Kretsinger, R. H., Analysis of the movements of helices in EF-hands. *Proteins* **2012**, *80* (11), 2592-600.
- 23. Tucker, M. J.; Oyola, R.; Gai, F., Conformational Distribution of a 14-Residue Peptide in Solution: A Fluorescence Resonance Energy Transfer Study. The Journal of Physical Chemistry B 2005, 109 (10), 4788-4795.